AJNR Am J Neuroradiol 26:1201–1206, May 2005

MR Imaging of Salivary Duct Carcinoma

Ken Motoori, Yumiko Iida, Yuichirou Nagai, Seiji Yamamoto, Takuya Ueda, Hiroyuki Funatsu, Hisao Ito, and Okamoto Yoshitaka

BACKGROUND AND PURPOSE: **Salivary duct carcinoma (SDC) is regarded as a high-grade malignancy in the current classification of salivary gland neoplasms. The aim of our study was to describe the MR imaging features of SDC.**

METHODS: **Nine patients with SDC underwent MR imaging study. The apparent diffusion coefficient (ADC) values of SDCs were measured from diffusion-weighted images. Time–signal intensity curves (TICs) of the tumors on dynamic MR images were plotted, and washout ratios were also calculated. TICs were divided into four types: type A, curve peaks <120 seconds after administration of contrast material with high washout ratio (≥30%); type B, curve peaks <120 seconds with low washout ratio (<30%); type C, curve peaks >120 seconds; type D, nonenhanced. We correlated the MR findings of SDC with the pathologic findings.**

RESULTS: **All tumors had ill-defined margins and showed low to moderately high signal intensity for contralateral parotid gland on T2-weighted images. The average of the ADC values of the SDCs was 1.16 ± 0.14 [SD] × 10^{-3}mm^2/s. Seven of nine (78%) tumors had type B enhancement. On the other hand, six of nine (67%) tumors with rich fibrotic tissue also had type C enhancement.**

CONCLUSION: **The findings of ill-defined margin, early enhancement with low washout ratio (type B), and low ADC value (1.22 × 10^{-3}mm^2/s) were useful for suggesting malignant salivary gland tumors. Although it was reported that type C enhancement was specific for pleomorphic adenoma, SDC frequently has type C-enhanced focus.**

Salivary duct carcinoma (SDC) is a rare, distinctive, and aggressive neoplasm of salivary glands. Structures of SDC are characterized by a striking resemblance to mammary duct carcinoma. Comedonecrosis is a frequent feature. SDC was first described by Kleinsasser et al (1) and was included in the recent World Health Organization classification (2). To the best of our knowledge, MR images of this rare entity have not been reported in the English-language literature. We present nine SDCs in parotid glands on MR images, including T1-weighted, T2-weighted, short-inversion-time inversion recovery (STIR), diffusion-weighted (DW), and dynamic contrast-enhanced MR (dynamic MR) images.

Methods

Subjects

Between May 2000 and January 2004, we encountered 12 SDCs, but three of them—carcinoma ex pleomorphic adenomas—were excluded. The nine patients with de novo SDC—seven men and two women with a mean age of 62 years (range, 37–83 years)—underwent MR imaging. Eight of them had a palpable hard mass in the parotid gland, and one had a hard mass in the submandibular gland. Of the eight patients with parotid tumors, two (25%) complained of parotid pain and six (75%) suffered ipsilateral facial nerve palsy.

MR Imaging Techniques

All MR examinations were performed by using 1.5T MR imaging units (GE Medical Systems, Milwaukee, WI) with a neurovascular array coil. T1-weighted images (400–500/9–14 [TR, ms/TE, ms]), T2-weighted images (4000/104, 16 [echo train length]), STIR images (4000/30, 12 [echo train length], 150 [TI, ms]), DW images (spin-echo single-shot echo-planar sequence with b factors of 0 and 1000 s/mm^2) were obtained at a section thickness of 6 mm, an intersection gap of 1 mm, an acquisition matrix of 256 × 256 (128 × 128 on DW images), and a field of view (FOV) of 22 × 22 cm. Dynamic MR images were obtained by 3D fat-suppression T1-weighted multiphase spoiled gradient-recalled-echo (6.3/1.4 [TR, ms/TE, ms]) for 4 minutes, with each phase lasting 27 seconds followed by a 3-second interval, an effective section thickness of 4 mm, FOV of 22 × 22 cm, and an acquisition matrix of 256 × 224. After the first set was obtained, contrast material injection was started immediately. Gadodiamide hydrate (Omniscan, Daiichi Pharmaceutical, Tokyo, Japan) was administered (0.2 mL/kg body weight) at a rate of 2.0 mL/s followed by a 20-mL saline flush into the antecubital vein. Seven sets of dynamic MR images were obtained serially. Soon after the dynamic MR imaging, fat-suppression T1-weighted images (340–400/20 [TR, ms/TE, ms]) were obtained with an acquisition matrix of

Received March 30, 2004; accepted after revision September 12.

From the Departments of Radiology (K.M., S.Y., T.U., H.F., H.I.) and Otolaryngology (Y.I., O.Y.), Chiba University Hospital, and the Department of Molecular Pathology (Y.N.), Chiba Postgraduate School of Medicine, Chiba City, Chiba, Japan.

Address correspondence to Ken Motoori, MD, Department of Radiology, Chiba University Hospital, 1-8-1, Inohana, Chuo-ku, Chiba City, Chiba, Japan.

256 × 224. Apparent diffusion coefficient (ADC) maps were automatically constructed from DW images. T1-weighted, STIR, gadolinium-enhanced dynamic images, and fat-suppression contrast-enhanced, T1-weighted images were obtained from all nine cases of SDC. T2-weighted images were obtained from six cases and DW images from seven cases.

Images and Pathologic Analysis

One radiologist (T.U.) measured the signal intensities of the lesions on each dynamic image with an electronic cursor to define the region of interest in each patient. Where markedly heterogeneous enhancement was seen, multiple regions of interest were obtained. TICs were then plotted from signal intensity values obtained for the tumors, the ipsilateral artery, and the ipsilateral vein. Washout ratio was calculated by a modified method of that of Yabuuchi et al (3) as follows:

$$[(SI_{max}-SI_{last})/(SI_{max}-SI_{pre})] \times 100\%,$$

where SI_{max} was the signal intensity at maximal contrast enhancement, SI_{last} the signal intensity at the last serial image of the dynamic study, and SI_{pre} the precontrast signal intensity. TICs were divided into four types according to those of Yabuuchi et al (3): type A, curve peaks <120 seconds after administration of contrast material with high washout ratio (≥30%); type B, curve peaks <120 seconds with low washout ratio (<30%); type C, curve peaks >120 seconds; type D, nonenhanced.

The ADC values of the SDCs were measured on each DW image with an electronic cursor to define the region of interest. The ADC values of the spinal cord on DW images were also measured to assess the validity of our method and to compare our findings with the results from previous investigations. The tumors were marked at the top during surgery. For MR images, they were cut on an axial plane. An experienced radiologist (K.M.) and a pathologist (Y.N.) correlated the findings from MR images and pathologic specimens. We attempted to identify the areas within the tumor as corresponding to hypointensity on STIR and T2-weighted images and also to identify each area corresponding to type A, B, and C curves on dynamic study.

Results

Eight SDCs occurred in parotid glands and one in the submandibular gland. The average maximal cross-sectional diameter was 3.7 cm (range, 2.2–5.2 cm). All tumors showed invasive or ill-defined margins on T1-weighted, T2-weighted, STIR, and contrast-enhanced T1-weighted images (Fig 1A–C). On T1-weighted images, all tumors showed hypointensity for parotid gland and isointensity for muscle (Fig 1C). On T2-weighted and STIR images, all tumors showed low to moderately high signal intensity for contralateral parotid gland (Fig 1A and B). The signal intensities of the tumors on T2-weighted images were lower than those of the tumors on STIR images (Fig 1A and B). There was no focus that showed higher signal intensity than that of cerebral spinal fluid on STIR and T2-weighted images.

On dynamic MR images, the artery curve peaked at 3–30 seconds after the administration of contrast agent and the vein curve peaked at 33–60 seconds. Three of the nine (33%) SDCs showed homogeneous enhancement and six of nine (67%) showed heterogeneous enhancement (Table): homogeneously enhanced SDCs, type B in two cases and type C in one case; and heterogeneously enhanced SDCs, type A plus B plus C in one case (Fig 1), type B plus C in three cases, type B plus C plus D in one case, and type B plus D in one case.

All DW images of SDCs showed irregularly high signal intensities. The average of the ADC values of the SDCs was 1.16 ± 0.14 [SD] × 10^{-3}mm^2/s (range of ADC values, 1.03–1.43), and that a range of ADC values of spinal cord was 1.05 ± 0.06 [SD] × 10^{-3}mm^2/s (0.99–1.15).

Specific cervical lymph nodes >10 mm in minimal axial diameter were found in five cases. Two of the five had irregularly enhanced lymph nodes on contrast-enhanced, fat-suppression T1-weighted images. Nonspecific cervical lymph nodes <10 mm were found in three cases. We could not detect cervical lymph nodes in one case.

Correlations between Radiologic and Pathologic Findings

All tumors had incomplete capsules and invasive borders. The light-optic appearance of the carcinomas resembled that seen in ductal carcinoma of the breast. Architectures of the tumor cells were variable in each case, including solid, papillary, micropapillary, cribiform, and infiltrative patterns. Many tumors had central desmoplasia (Fig 1). The pattern of enhancement on dynamic MR images in central desmoplastic areas was gradual upward enhancement (type C). The area also showed iso- to hypointensity on STIR and T2-weighted images. In the peripheral zones of the tumors, fibrosis, necrosis, comedonecrosis, tumor cells, and lymphoplasmacytic infiltration were mixed at various proportions. The combinations were slightly different in each case. The various proportions resulted in a variety of TICs on dynamic MR images: type A, cellular component-dominant area showing early enhancement and high washout ratio (Fig 1G); type B, cellular components with many necrotic foci and fibrosis showing early enhancement with poor washout (Fig 1H); and type C, abundant fibrotic tissue with few cellular components showing gradual upward enhancement (Fig 1I).

Pathologically, five of nine (55.6%) SDCs had metastatic lymph nodes. Four of the five cases with lymph nodes >10 mm in minimal axial diameter were positive, and the other showed reactive change. All cases with smaller lymph nodes were negative. One case without detectable cervical lymphadenopathy had metastatic lymph nodes that were involved in the primary tumor. Reactive lymph nodes showed type A curve on dynamic study. In a case of left parotid SDC with ipsilateral metastatic lymphadenopathies, a metastatic lymph node showed type B curve and a contralateral reactive lymph node showed type A curve (Fig 2). The ADC value of the metastatic lymph node (1.23 × 10^{-3}mm^2/s) was higher than that of the reactive lymph node (0.90 × 10^{-3}mm^2/s). Reactive lymph nodes possessed the whole normal lymph node structures without the size. Malignant cells were involved in the metastatic lymph nodes, which also contained microscopic necrotic foci, hemorrhagic changes, and reactive fibrosis. Macrosopic necrosis showed hypointensity on contrast-enhanced, fat-suppression T1-weighted imaging.

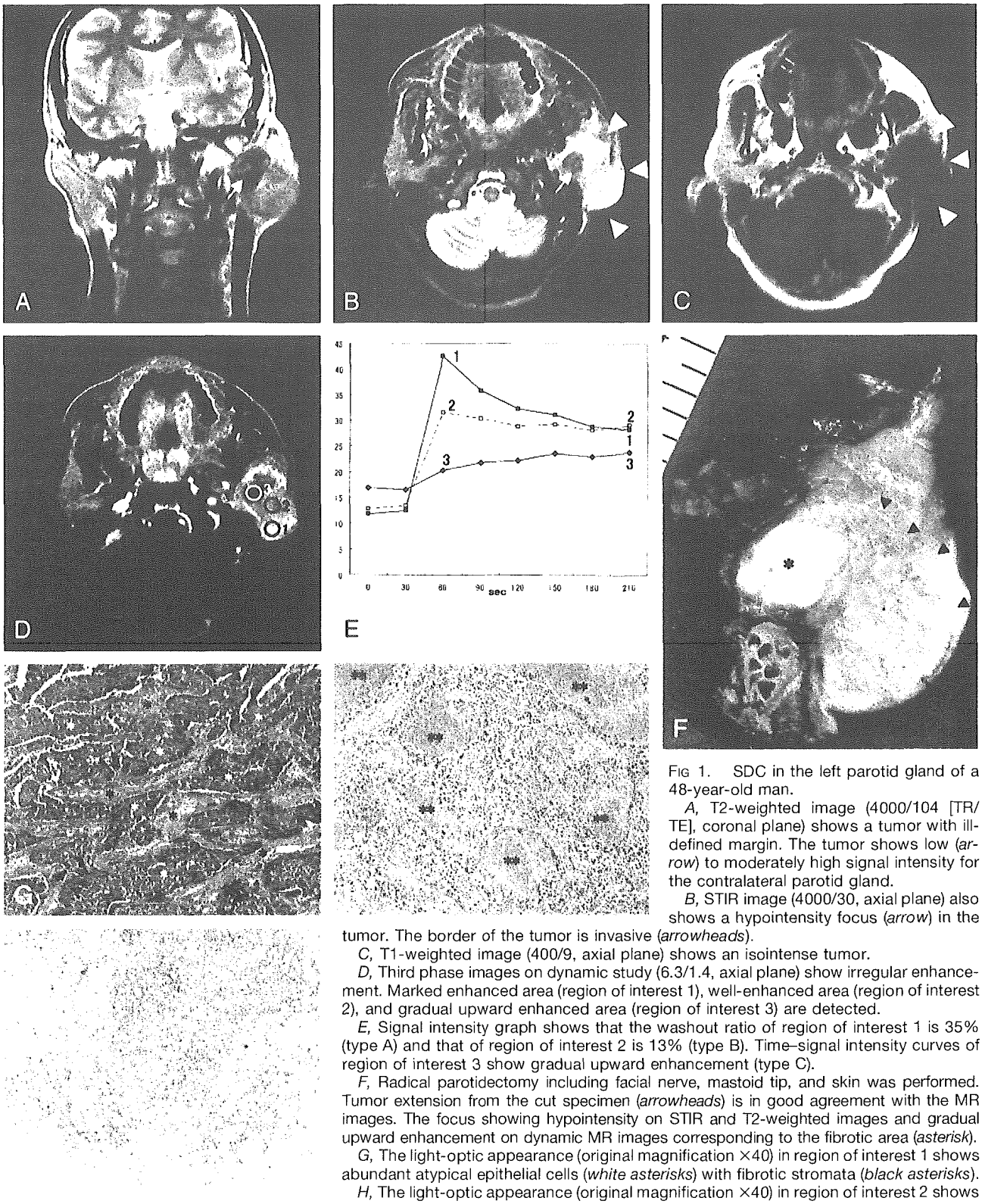

FIG 1. SDC in the left parotid gland of a 48-year-old man.

A, T2-weighted image (4000/104 [TR/TE], coronal plane) shows a tumor with ill-defined margin. The tumor shows low (*arrow*) to moderately high signal intensity for the contralateral parotid gland.

B, STIR image (4000/30, axial plane) also shows a hypointensity focus (*arrow*) in the tumor. The border of the tumor is invasive (*arrowheads*).

C, T1-weighted image (400/9, axial plane) shows an isointense tumor.

D, Third phase images on dynamic study (6.3/1.4, axial plane) show irregular enhancement. Marked enhanced area (region of interest 1), well-enhanced area (region of interest 2), and gradual upward enhanced area (region of interest 3) are detected.

E, Signal intensity graph shows that the washout ratio of region of interest 1 is 35% (type A) and that of region of interest 2 is 13% (type B). Time–signal intensity curves of region of interest 3 show gradual upward enhancement (type C).

F, Radical parotidectomy including facial nerve, mastoid tip, and skin was performed. Tumor extension from the cut specimen (*arrowheads*) is in good agreement with the MR images. The focus showing hypointensity on STIR and T2-weighted images and gradual upward enhancement on dynamic MR images corresponding to the fibrotic area (*asterisk*).

G, The light-optic appearance (original magnification ×40) in region of interest 1 shows abundant atypical epithelial cells (*white asterisks*) with fibrotic stromata (*black asterisks*).

H, The light-optic appearance (original magnification ×40) in region of interest 2 shows atypical epithelial cells (*white asterisks*) with fibrotic stromata and many foci of comedonecrosis (*double asterisks*).

I, The light-optic appearance (original magnification ×40) in region of interest 3 shows dense fibrotic tissue with cellular components (*white asterisk*).

Discussion

SDC is a high-grade malignancy occurring predominantly in the major salivary glands of older male patients (4–14). SDC is frequently diagnosed at an advanced stage; in our study, 75% of the patients had facial nerve palsy and 50% of SDCs had already spread to cervical lymph nodes. Surgery and postoperative radiation therapy was the treatment of choice.

MR features of 9 patients with salivary duct carcinoma

Patient	Age (yr)	Sex	Site	Size (cm)	LNs	TICs			ADC Value ($\times 10^{-3}$ mm^2/s)
1	53	M	rt parotid	3.2	Yes	B (11–25)	C		
2	81	M	rt parotid	2.1	No	B (22)	C		
3	37	M	rt parotid	3.4	Yes	B (11)	C	D	1.03
4	65	F	rt parotid	4.0	No	B (12)	D		1.06
5	83	M	rt parotid	3.4	No	C			1.43
6	52	M	lt parotid	3.8	Yes	B (27)	C		1.15
7	60	M	rt parotid	2.1	Yes	B (1)			1.20
8	48	M	lt parotid	4.5	No	A (35)	B (13)	C	1.18
9	83	F	lt submandibular	2.8	Yes	B (19)			1.05

Note.—LNs indicates lymph nodes, TICs, time-signal intensity curves, Washout ratio (WR) in parentheses, expressed as percentage.

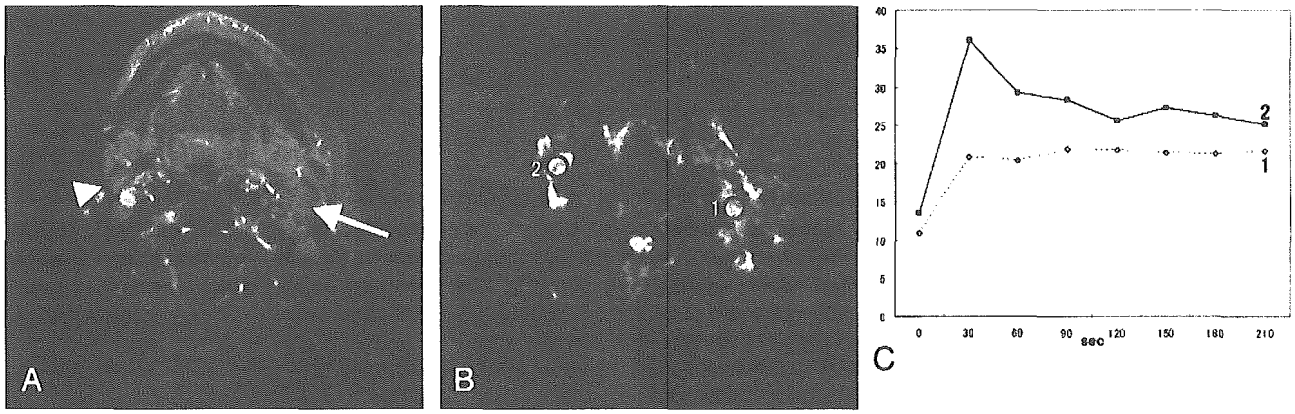

FIG 2. SDC in the left parotid gland of a 52-year-old man. He has ipsilateral metastatic lymph nodes and contralateral reactive lymph nodes.

A, Fat-suppression T1-weighted image (340/20, axial plane) shows multiple cervical lymphadenopathies. Metastatic lymph node (*arrow*) is >10 mm in minimal axial diameter. Reactive lymph node (*arrowhead*) is <10 mm in minimal axial diameter.

B, On diffusion-weighted image (spin-echo single-shot echo-planar sequence with b factors of 0 and 1000 s/mm^2), both lymph nodes show high signal intensity. The ADC value of the metastatic lymph node (region of interest 1) is 1.23 × 10^{-3} mm^2/s and that of the reactive lymph node is 0.90 × 10^{-3} mm^2/s.

C, Signal intensity graph shows that the washout ratio of region of interest 1 is 2% (type B) and that of region of interest 2 is 48% (type A).

Despite this aggressive treatment, most patients died within 2–3 years. Local recurrence in SDC has been reported in 16–55% of the cases (9–14). Although local recurrence in this tumor, as well as neck recurrence, is very frequent, it does not present a major clinical problem. Distant metastases are the most common cause of death. Distant spread is related to the presence of metastatic lymph nodes rather than T categories (14). Wide local resection and prophylactic ipsilateral neck dissection have a possible preventive role in distant spread (14). MR imaging is an established and useful way of demonstrating the morphology and extent of head and neck tumors, as well as their relationship with adjacent structures. If, however, MR imaging could make a suggestion of SDC as one of differential diagnosis, its role would have an added value.

SDC is composed of atypical epithelial cells arranged in varying proportions of cribriform, papillary, micropapillary, or solid growth patterns with fibrotic stromata. Comedonecrosis is present in most cases. Perineural, venous, and lymph duct invasions are also common findings. In our study, SDCs had dense fibrosis in the center. On the other hand, in the peripheral zone of the tumors, fibrosis, necrosis, comedonecrosis, tumor cells, and lymphoplasmacytic infiltration were at various proportions. Hypointensity on STIR and T2-weighted images and gradual upwardly enhanced foci on dynamic MR images corresponded to the areas with desmoplasia. According to Yabuuchi et al (3), in a study including 22 benign and 11 malignant tumors, gadolinium-enhanced dynamic MR imaging was useful for predicting whether salivary gland tumors were benign or malignant. They reported that a short time of peak enhancement, <120 seconds, and a low washout ratio, <30% (type B), on dynamic MR images were useful criteria for the diagnosis of malignant tumor. They also reported that a gradual upward enhanced tumor (type C) was pleomorphic adenoma. According to Tsushima et al (15), pleomorphic adenoma and adenoid cystic carcinoma showed gradual upward enhancement. In their study of malignant parotid tumors, except for adenoid cystic carcinoma, three squamous cell carcinomas, two mucoepidermoid carcinomas, one lymphoma, and one acinic cell carcinoma showed early enhancement. In our study, eight of nine (89%) tumors presented an enhancement pattern of malignancy: pure type B in

two cases, type B plus C in three cases, type B plus D in one case, type B plus A plus C in one case, and type B plus C plus D in one case. On the other hand, six of nine (67%) tumors had a gradual upwardly enhanced pattern (type C): pure type C in one case, type C plus B in three cases, type C plus A plus B in one case, and type C plus B plus D in one case. The gradual enhancement of pleomorphic adenoma corresponds to myxoid stromata (16). Adenoid cystic carcinomas also have rich interstitial space filled with mucin (15). Myxoid stromata and mucin show high signal intensity on STIR and T2-weighted images (16, 17). The gradual enhanced focus of SDC corresponding to desmoplasia is iso- to hypointense to surrounding structures on STIR and T2-weighted images. Structures of SDC are characterized by a striking resemblance to mammary duct carcinoma. In a case of invasive ductal carcinoma, the central portion of the tumor showed gradual upward enhancement on dynamic MR images because of the low density of microvessels in this region, which is associated with prominent fibrosis (18). Fibrosis can be differentiated from myxoid stromata on the basis of signal intensity characteristics on STIR and T2-weighted images.

According to Wang et al (19), an ADC value $<1.22 \times 10^{-3}mm^2/s$ was one of the criteria for predicting malignancy. In our study, the average ADC values of SDC (1.16 ± 0.14 [SD] $\times 10^{-3}mm^2/s$) agreed well with their data. One tumor showed a slightly high ADC value ($1.43 \times 10^{-3}mm^2/s$); this tumor had abundant microscopic necrotic foci, but they could not be detected on MR images. There was a possibility that these many microscopic necroses were the cause of the elevated ADC value. Usually, the mean ADC value of cystic and necrotic components is higher than that of cellular tissue, because the mobility of water protons is relatively freer in fluid than in other tissues.

MR imaging also has the task of identifying gross metastatic cervical lymphadenopathy. Metastasis was suggested if a cervical lymph node was >10 mm in minimal axial diameter (20). Irregular enhancement on contrast-enhanced, fat-suppression T1-weighted imaging was also suggestive of metastatic lymph nodes (21). In our study, four of five pathologically positive cases and one of four pathologically negative cases had lymph nodes >10 mm in minimal axial diameter. In a false-negative case, metastatic lymph nodes could not be detected because of involvement in the primary tumor. In a false-positive case (Fig 2), although metastasis was suggested because of the size of the minimal axial diameter, the type A curve of TIC on dynamic study was atypical for metastasis. The type A curve is a criterion standard for a benign lesion (3). In the case of left SDC with ipsilateral metastatic lymphadenopathies (Fig 2), a metastatic lymph node showed a type B curve and a contralateral reactive lymph node showed a type A curve, and the ADC value of the metastatic lymph node was higher than that of the reactive lymph node (1.23 vs $0.90 \times 10^{-3}mm^2/s$). In our study, the average ADC value of SDCs (1.16 ± 0.14 [SD] $\times 10^{-3}mm^2/s$ [1.03–1.43]) was higher than that of spinal cord (1.05 ± 0.06 [SD] $\times 10^{-3}mm^2/s$ [0.99–1.15]). According to Wang et al (18), the ADC value of malignant lymphoma (0.66 ± 0.17 [SD] $\times 10^{-3}$ mm^2/s) is lower than that of spinal cord. In the state of hypercellularity with less extracellular space as seen in lymphoma, the mobility of water protons is relatively limited. Thus, it was not surprising that the reactive lymph node showed a low ADC value. Microscopic necrosis and hemorrhagic changes caused the ADC values of metastatic lymph nodes to be higher than those of reactive lymph nodes. The size criterion for cervical lymph node metastasis, 10 mm or more in minimal axial diameter, showed 80% sensitivity and 75% specificity. Combining the information of type B curve on dynamic study and the approximate ADC value to primary tumor strongly suggested metastatic lymph nodes. This information improved sensitivity from 80% to 100% and specificity from 75% to 80%.

Conclusion

The current series shows that various MR imaging findings correlated well with the pathologic findings of SDC. The findings of ill-defined margin, early enhancement with low washout ratio (type B) on dynamic MR images, and low ADC value ($1.22 \times 10^{-3}mm^2/s$) were useful for suggesting malignant salivary gland tumors. Although it was reported that gradual upward enhancement (type C) was specific for pleomorphic adenoma, SDC frequently has a type C enhanced focus. The gradual enhanced foci of pleomorphic adenoma showed marked high intensity on STIR and T2-weighted images, a feature associated with myxoid stromata. On the other hand, the gradual enhanced foci of SDC had prominent fibrosis and showed lower signal intensity on STIR and T2-weighted images. The focus in SDC that shows gradual upward enhancement on dynamic MR images and hypointensity on STIR and T2-weighted images may be a clue for making a diagnosis of SDC and separating SDC from the more common malignant salivary gland tumors such as mucoepidermoid carcinoma and adenoid cystic carcinoma.

References

1. Kleinsasser O, Klein HJ, Hubner G. **Speichelgangcarcinomas: Ein den Milchgangcarcinomen der Brustdruse Analoge Gruppe von Speicheldrusentumoren.** *Arch Klin Exp Ohren Nasen Kehlkopfheikd* 1968;192:100–105
2. Seifert G, Sobin LH. *Histological Typing of Salivary Gland Tumors: World Health Organization International Histological Classification of tumors.* 2nd ed. New York: Springer-Verlag;1991
3. Yabuuchi H, Fukuya T, Tajima T, et al. **Salivary gland tumors: diagnostic value of gadolinium-enhanced dynamic MR imaging with histopathologic correlation.** *Radiology* 2003;226:345–354
4. Chen KT, Hafez GR. **Infiltrating salivary duct carcinoma: a clinicopathologic study of five cases.** *Arch Otolaryngol* 1981;107:37–39
5. Chen KT. **Intraductal carcinoma of the minor salivary gland.** *J Laryngol Otol* 1983;97:189–191
6. Garland TA, Innes DJ Jr., Fechner RE. **Salivary duct carcinoma: an analysis of four cases with review of literature.** *Am J Clin Pathol* 1984;81:436–441
7. Hui KK, Batsakis JG, Luna MA, et al. **Salivary duct adenocarcinoma: a high grade malignancy.** *J Laryngol Otol* 1986;100:105–114

8. Anderson C, Muller R, Piorkowski R, et al. **Intraductal carcinoma of major salivary gland.** *Cancer* 1992;69:609–614
9. Afzelius LE, Cameron WR, Svensson C. **Salivary duct carcinoma: a clinicopathologic study of 12 cases.** *Head Neck Surg* 1987;9:151–156
10. Brandwein MS, Jagirdar J, Patil J, et al. **Salivary duct carcinoma (cribriform salivary carcinoma of excretory ducts): a clinicopathologic and immunohistochemical study of 12 cases.** *Cancer* 1990;65:2307–2314
11. Colmenero Ruiz C, Patron Romero M, Martin Perez M. **Salivary duct carcinoma: a report of nine cases.** *J Oral Maxillofac Surg* 1993;51:641–646
12. Delgado R, Vuitch F, Albores-Saavedra J. **Salivary duct carcinoma.** *Cancer* 1993;72:1503–1512
13. Martinez-Barba E, Cortes-Guardiola JA, Minguela-Puras A, et al. **Salivary duct carcinoma: clinicopathological and immunohistochemical studies.** *J Craniomaxillofac Surg* 1997;25:328–334
14. Guzzo M, Di Palma S, Grandi C, Molinari R. **Salivary duct carcinoma: clinical characteristics and treatment strategies.** *Head Neck* 1997;19:126–133
15. Tsushima Y, Matsumoto M, Endo K. **Parotid and parapharyngeal tumours: tissue characterization with dynamic magnetic resonance imaging.** *Br J Radiol* 1994;67:342–345
16. Motoori K, Yamamoto S, Ueda T, et al. **Inter- and intratumoral variability in magnetic resonance imaging of pleomorphic adenoma.** *J Comput Assist Tomogr* 2004;28:233–246
17. Tsushima Y, Matsumoto M, Endo K, et al. **Characteristic bright signal of parotid pleomorphic adenomas on T2-weighted MR images with pathological correlation.** *Clin Radiol* 1994;49:485–489
18. Buadu LD, Murakami J, Murayama S, et al. **Breast lesions: correlation of contrast medium enhancement patterns on MR images with histopathologic findings and tumor angiogenesis.** *Radiology* 1996;200:639–649
19. Wang J, Takashima S, Takayama F, et al. **Head and neck lesions: characterization with diffusion-weighted echo-planar MR imaging.** *Radiology* 2001;220:621–630
20. van den Brekel MW, Stel HV, Castelijns JA, et al. **Cervical lymph node metastasis: assessment of radiologic criteria.** *Radiology* 1990;177:379–384
21. Som PM. **Detection of metastasis in cervical lymph nodes: CT and MR criteria and differential diagnosis.** *AJR Am J Roentgenol* 1992; 158:961–969

Identification of Warthin Tumor

Magnetic Resonance Imaging Versus Salivary Scintigraphy With Technetium-99m Pertechnetate

Ken Motoori, MD, Takuya Ueda, MD,* Yoshitaka Uchida, MD,* Hideaki Chazono, MD,† Homare Suzuki, MD,† and Hisao Ito, MD**

Objective: The aim of this study was to evaluate the accuracy of technetium-99m (Tc-99m) pertechnetate scintigraphy and magnetic resonance (MR) imaging in the diagnosis of Warthin tumor.

Methods: Sixteen cases of Warthin tumor and 17 cases of non-Warthin tumor were examined by Tc-99m pertechnetate scintigraphy with lemon juice stimulation and MR imaging, including T1-weighted, T2-weighted, short inversion time inversion recovery, diffusion-weighted, and contrast-enhanced dynamic images. We used the receiver operating characteristic (ROC) curve to evaluate diagnostic accuracy.

Results: The mean area under the ROC curves of MR imaging in the diagnosis of Warthin tumor (0.97) was higher than that of Tc-99m pertechnetate scintigraphy (0.88).

Conclusion: Magnetic resonance imaging is more useful in the evaluation of Warthin tumor than Tc-99m pertechnetate scintigraphy.

Key Words: Warthin tumor, parotid gland, magnetic resonance imaging, salivary gland scintigraphy

(*J Comput Assist Tomogr* 2005;29:506–512)

It is well known that technetium-99m (Tc-99m) pertechnetate is a simple and noninvasive useful method for the diagnosis of Warthin tumor.[1–7] The enhanced usefulness of Tc-99m pertechnetate scintigraphy after lemon juice stimulation in Warthin tumor has also been reported.

Imaging of the parotid glands has 2 purposes: the first is to evaluate the precise extent and site of a parotid lesion, and the second is to provide some indication of its pathologic nature. It is important to determine whether a parotid gland tumor is benign or malignant and to assess its extent and relation to adjacent structures before surgery, because this information strongly influences the choice of surgical procedure. Benign tumors undergo local excision or superficial parotidectomy, whereas total parotidectomy with or without facial nerve removal is performed for malignant tumors.[8,9] The pathologic diagnosis is typically determined by fine needle aspiration cytology. Thus, although it seems that there should be an important role for preoperative imaging, its clinical significance is relatively minor in reality. Although fine needle aspiration cytology is the most cost-effective and minimally invasive way to determine the histology of a parotid tumor, fine needle aspiration cytology is not always conclusive, because specimen material from a small or deep mass may be insufficient.[10–12] Magnetic resonance (MR) imaging is a useful and established way, rather than Tc-99m pertechnetate scintigraphy, to demonstrate the morphology and extent of head and neck tumors as well as their relation to adjacent structures. If, however, MR imaging could make a reliable distinction between Warthin tumor and other parotid tumors, including malignant neoplasms, its role and importance in diagnostics would become considerably enhanced. The purpose, then, of this study was to evaluate the accuracy of Tc-99m pertechnetate scintigraphy and MR imaging in the diagnosis of Warthin tumor.

MATERIALS AND METHODS

Subjects

The patient group, consisting of 33 individuals with parotid tumors or suspected Warthin tumors, underwent MR and Tc-99m pertechnetate imaging before surgery or fine needle aspiration cytology between April 2000 and April 2004. The group was composed of 26 male and 7 female patients, ranging in age from 16 to 91 years (mean = 60.8 years). All tumors were all pathologically proven and consisted of 16 Warthin tumors, 9 pleomorphic adenomas, 3 reactive lymphadenopathies, and 5 malignant parotid tumors (2 acinic cell carcinomas, 1 adenocarcinoma, 1 squamous cell carcinoma, and 1 malignant lymphoma).

Technetium-99m Scans

Approximately 5 minutes after the intravenous injection of 185–370 MBq Tc-99m, static spot images in the anterior and bilateral positions were obtained with a double-head gamma camera (PRISM 2000XP; Picker International, Cleveland, OH) with a low-energy and high-resolution collimator. Images were acquired at a rate of 300 seconds per frame. Late images were obtained in 3 positions before and

Received for publication November 30, 2004; accepted March 24, 2005.
From the *Department of Radiology, Chiba University Hospital, Chiba City, Chiba, Japan, and †Department of Otolaryngology, Chiba University Hospital, Chiba City, Chiba, Japan.
Reprints: Ken Motoori, Department of Radiology, Chiba University Hospital, 1-8-1, Inohana, Chuo-ku, Chiba City, Chiba, Japan (e-mail: motoorik@faculty.chiba-u.jp).

after the salivary glands were stimulated with 100 mg citric acid or lemon juice.

MR Imaging Techniques

The MR apparatus was a 1.5-T MR unit (General Electric Medical Systems, Milwaukee, WI) with a neurovascular array coil. T1-weighted images (repetition time/echo time [TR/TE]: 400–500 milliseconds/9–14 milliseconds) of the transverse plane, short inversion time inversion recovery (STIR) images (TR/TE: 4000 milliseconds/30 milliseconds, echo train length = 12, inversion time = 150 milliseconds) of the same transverse plane as the T1-weighted images, diffusion-weighted (DW) images (spin echo single-shot echo planar sequence with b factors of 0 and 1000 mm^2/s) of the same transverse plane, and T2-weighted spin echo images (TR/TE: 4000 milliseconds/104 milliseconds, echo train length = 16) of the same transverse or coronal plane were obtained at a section thickness of 6 mm, an intersection gap of 1 mm, an acquisition matrix of 256 × 256 (128 × 128 on DW images), and a field of view of 22 cm × 22 cm. Dynamic contrast-enhanced MR images were obtained by 3-dimensional, fat-suppression, T1-weighted, multiphase, spoiled gradient recalled echo imaging (TR/TE: 6.3 milliseconds/1.4 milliseconds) for 4 minutes. Seven sets of dynamic contrast-enhanced images were obtained serially, with an effective section thickness of 4 mm, a field of view of 22 cm × 22 cm, and an acquisition matrix of 256 × 224. After the first set was obtained, contrast material injection was started immediately. Gadodiamide hydrate (Omniscan; Daiichi Pharmaceutical Corporation, Tokyo, Japan) was administered (0.2 mL/kg of body weight) at a rate of 2.0 mL/s, followed by a 20-mL saline flush into the antecubital vein. Soon after the dynamic contrast-enhanced MR imaging, fat-suppression T1-weighted images (TR/TR: 340–400 milliseconds/20 milliseconds) of the same transverse plane as the

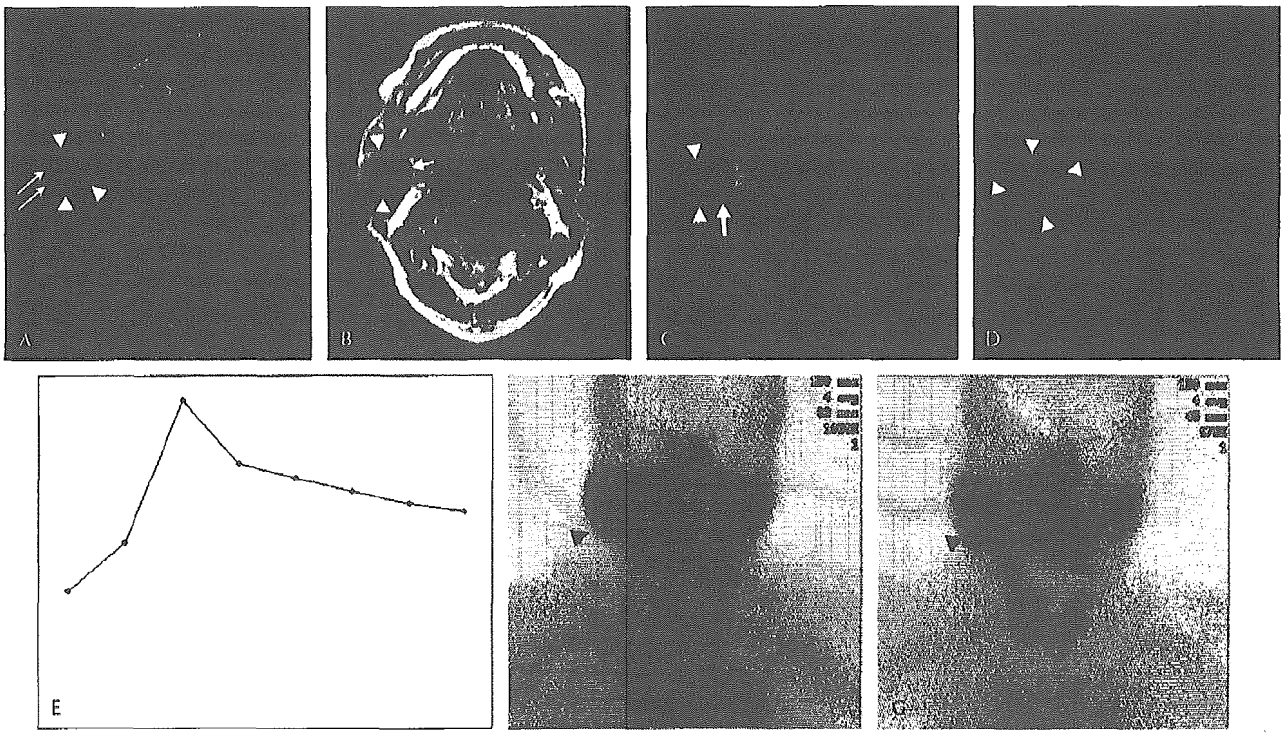

FIGURE 1. Warthin tumor in a 72-year-old man. A, Short inversion time inversion recovery image (repetition time/echo time [TR/TE]: 4000 milliseconds/30 milliseconds, axial plane) shows a well-defined lesion in the inferior pole of the right parotid gland (arrowheads). The lateral half of the lesion has characteristic hypointensity components (arrows). B, On T1-weighted imaging (TR/TE: 400 milliseconds/9 milliseconds, axial plane), the lateral half of the lesion shows high intensity (arrowheads) to muscles and the medial half shows isointensity (arrow). C, On diffusion-weighted imaging (b factor = 1000 seconds/mm^2), the lateral side of the lesion shows heterogeneous high intensity (arrowheads) and the medial side shows homogeneous high intensity (arrow). The automatically constructed apparent diffusion coefficient (ADC) map reveals an ADC value of the medial half of the lesion of 0.96 × 10^{-3} mm^2/s, which is lower than that of the cervical spinal cord (1.02 × 10^{-3} mm^2/s). D, On fat-suppression, contrast-enhanced, T1-weighted imaging (TR/TE: 300 milliseconds/20 milliseconds, coronal plane), the lesion shows heterogeneous enhancement (arrowheads). E, Time-signal intensity curve, plotted from signal intensity values obtained for the medial half of the lesion on dynamic magnetic resonance imaging, shows early enhancement and a high washout ratio (58%). The lateral side of the lesion shows poor enhancement. This suggests that the area has hemorrhagic degeneration. F, Early technetium-99m pertechnetate image shows increased uptake in the inferior portion of the right parotid gland (arrowhead) corresponding to the left parotid gland. G, Late image with lemon juice stimulation also shows increased uptake in the same portion (arrowhead).

precontrast enhanced T1-weighted images or the coronal plane were obtained with an acquisition matrix of 256 × 224. Apparent diffusion coefficient (ADC) maps were automatically constructed from DW images.

Image Analysis

Salivary scintigraphy and MR images were interpreted retrospectively by 2 readers (T.U. [11 years of experience] and Y.U. [17 years of experience]) who were blinded to identification of the patients. The readers knew that all patients were suspected of having parotid tumors. At first, salivary scintigrams were interpreted. The criterion for detecting Warthin tumor was a higher uptake focus on Tc-99m pertechnetate scintigraphy after citric acid or lemon juice stimulation.[1,2] On the basis of the findings, the possibility of Warthin tumor was estimated by the readers using a 5-point rating scale: 1, definitely or almost definitely absent; 2, probably absent; 3, possibly present; 4, probably present; and 5, definitely or almost definitely present. The possibility of malignancy was also estimated by the readers using a 5-point scale.

More than 2 weeks after the first reading, the 2 readers reviewed MR images, including T1-weighted, T2-weighted, STIR, and DW images and contrast-enhanced dynamic studies. The diagnostic clues of Warthin tumor on MR images are as follows.[13] Most Warthin tumors are revealed to involve the inferior pole of the parotid gland and to have a smooth margin on T1-weighted and T2-weighted imaging.[13] Warthin tumors sometimes show characteristic hypointensity areas on STIR and T2-weighted images (Fig. 1).[13] Warthin tumors show early enhancement and a high washout ratio (>30%) on dynamic MR images and a lower ADC value than that of the spinal cord on DW images.[13,14] A 30% washout ratio threshold is useful for predicting whether salivary gland tumors are benign or malignant (Fig. 2).[15,16] The diagnostic clue of pleomorphic adenoma is to find the myxoid component, which shows high intensity on STIR and T2-weighted images, progressive enhancement on dynamic MR images, and high ADC values on DW images (Fig. 3).[16] On the basis of the findings, the possibility of Warthin and malignant tumors was estimated by the readers using a 5-point rating scale similar to that of salivary scintigraphy.

Statistical Analysis

A binomial receiver operating characteristic (ROC) curve was fitted to each reader's confidence scoring. The diagnostic accuracy of each image set was determined by

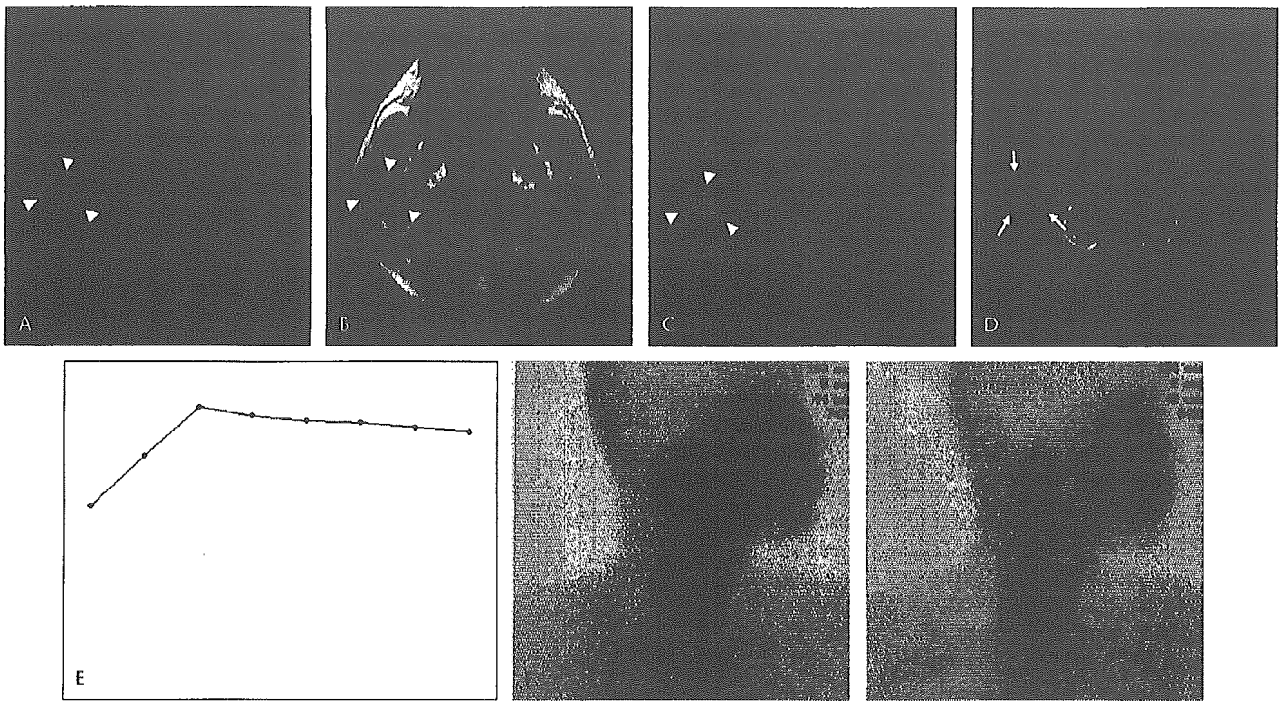

FIGURE 2. Acinic cell carcinoma in a 21-year-old man. A, Short inversion time inversion recovery image (repetition time/echo time [TR/TE]: 4000 milliseconds/30 milliseconds, axial plane) shows a well-circumscribed lesion in the deep lobe of the right parotid gland (arrowheads). The lesion shows moderately high intensity. B, On T1-weighted imaging (TR/TE: 340 milliseconds/9 milliseconds, axial plane), the lesion shows moderately high intensity to muscles (arrowheads). C, On diffusion-weighted imaging (b factor = 1000 seconds/mm^2), the lesion shows heterogeneous high intensity (arrowheads). The automatically constructed apparent diffusion coefficient (ADC) map reveals an ADC value of the lesion of 1.13×10^{-3} mm^2/s, which is slightly higher than that of the cervical spinal cord (0.997×10^{-3} mm^2/s). D, On fat-suppression, contrast-enhanced, T1-weighted imaging (TR/TE: 300 milliseconds/20 milliseconds, coronal plane), the lesion shows marginal enhancement (arrows). E, Time-signal intensity curve of the lesion shows early enhancement and a poor washout ratio (24%). F, G, Early and late images of technetium-99m pertechnetate show a cold area in the right parotid gland (*).

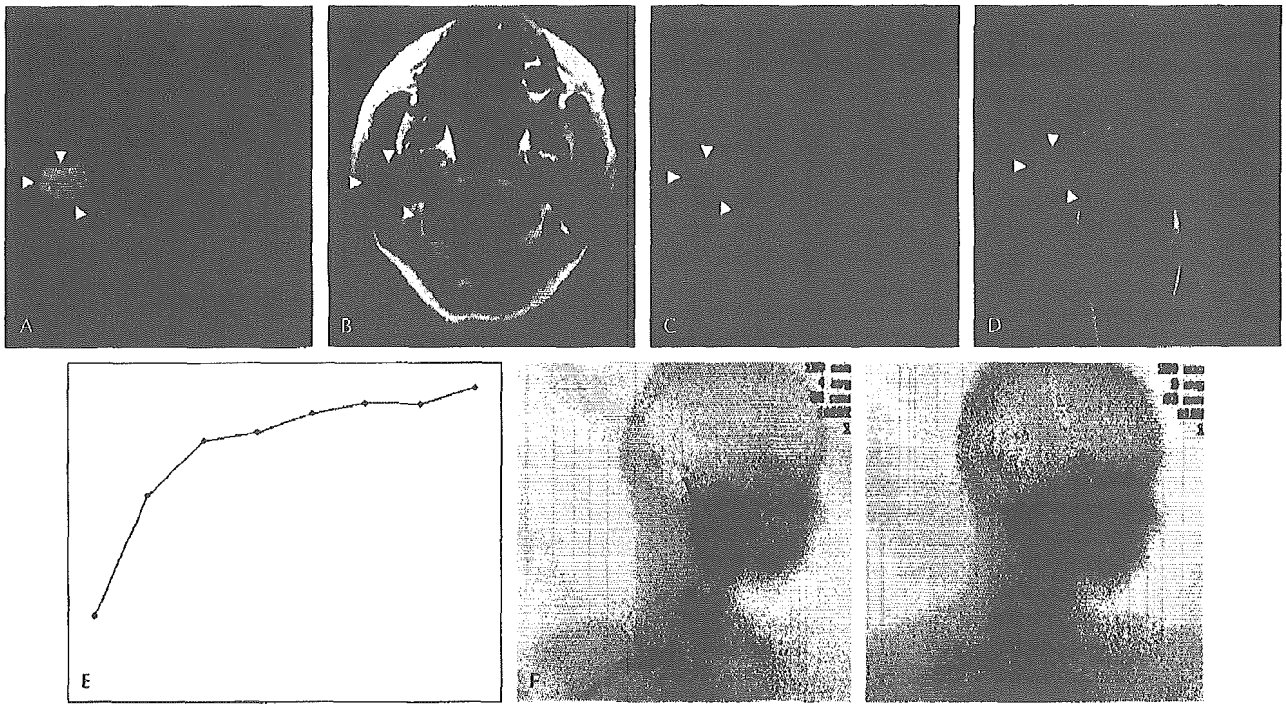

FIGURE 3. Pleomorphic adenoma in a 59-year-old woman. A, Short inversion time inversion recovery image (repetition time/echo time [TR/TE]: 4000 milliseonds/30 milliseconds, axial plane) shows a well-circumscribed markedly high-intensity lesion in the deep lobe of the right parotid gland (arrowheads). B, On T1-weighted imaging (TR/TR: 400 milliseconds/9 milliseconds, axial plane), the lesion shows isointensity to muscles (arrowheads). C, On diffusion-weighted imaging (b factor = 1000 seconds/mm^2), the lesion shows moderately high intensity (arrowheads). An automatically constructed apparent diffusion coefficient (ADC) map reveals an ADC value of the lesion of 1.81×10^{-3} mm^2/s, which is higher than that of the cervical spinal cord (0.982×10^{-3} mm^2/s). D, On fat-suppression, contrast-enhanced, T1-weighted imaging (TR/TE: 300 milliseconds/20 milliseconds, coronal plane), the lesion shows heterogeneous enhancement (arrowheads). E, Time-signal intensity curve of the lesion shows gradual upward enhancement. F, G, Early and late images of technetium-99m pertechnetate show a cold area in the right parotid gland (arrow).

calculating the area under each reader-specific binomial ROC curve (Az). The computer software for depicting ROC curves and for calculating Az values was the ROCKIT 0.9B beta version program (C. Metz, Chicago, IL). We obtained composite ROC curves that represented the overall performance of the readers using an averaging method. The differences between the 2 image sets in terms of mean Az values were analyzed statistically by the Student paired t test.

We also calculated sensitivity and specificity, positive predictive value, and negative predictive value in each reading session of each reader. The nodules scoring confidence levels of 4 and 5 were counted as positive, and those scoring 1 to 3 were counted as negative.

RESULTS

Four (25%) of 16 cases of Warthin tumor had cystic components, 4 (25%) of 16 cases were multifocal lesions, and the average tumor size of the Warthin tumor in the 16 cases was 2.7 ± 0.8 cm.

The readers attained a statistically higher Az value for the detection of Warthin tumors and malignant tumors in their interpretation of the MR imaging set compared with that of the salivary scintigram set (Tables 1, 2). No statistically significant difference could be identified between the readers in the reading sessions. The average Az values of the composite ROC curves of the salivary scintigram set and the MR imaging set for the detection of Warthin tumor were 0.88 and 0.97, respectively (Fig. 4), and for malignant tumors, they were 0.66 and 0.94, respectively (Fig. 5). In the salivary scintigram set, 5 Warthin tumors were scored as negative by both readers and

TABLE 1. Detection of Warthin Tumor

	Sensitivity	Specificity	PPV	NPV	Az
Results of Tc-99m pertechnetate scintigraphy reading session					
Reader 1	0.56	1.00	1.00	0.71	0.88
Reader 2	0.63	0.94	0.91	0.73	0.88
Results of MR imaging reading session					
Reader 1	0.94	0.88	0.88	0.94	0.97
Reader 2	0.75	0.94	0.92	0.80	0.96

NPV indicates negative predictive value; PPV, positive predictive value.

TABLE 2. Detection of Malignant Parotid Tumor

	Sensitivity	Specificity	PPV	NPV	Az
Results of Tc-99m pertechnetate scintigraphy reading session					
Reader 1	0.40	0.71	0.20	0.87	0.67
Reader 2	0.20	0.89	0.25	0.86	0.64
Results of MR imaging reading session					
Reader 1	0.60	1.00	1.00	0.93	0.96
Reader 2	0.80	0.96	0.80	0.96	0.92

NPV indicates negative predictive value; PPV, positive predictive value.

3 Warthin tumors had different scoring levels between the 2 readers. In the MR imaging set, there were no Warthin tumors scored as negative by both readers but 5 Warthin tumors had different scoring levels between the 2 readers.

The average size of Warthin tumors counted as nodules scoring confidence levels of 1 to 3 in interpretation of the salivary scintigram set was 25 ± 10 mm, and 3 (43%) of 7 had big cysts. The average size of these low-grade uptake tumors, excluding large cystic components, was 20 ± 7 mm. That of Warthin tumors counted as nodules scoring confidence levels of 4 or 5 in interpretation of the salivary scintigram set was 29 ± 6 mm, and none of them had big cystic components, although 1 had a small cyst.

One case of intraparotid lymphadenopathy was misdiagnosed as Warthin tumor in interpretation of the MR imaging set (Fig. 6), and 1 acinic cell carcinoma was also misdiagnosed as a benign tumor because of its smooth margin and high washout ratio (33%).

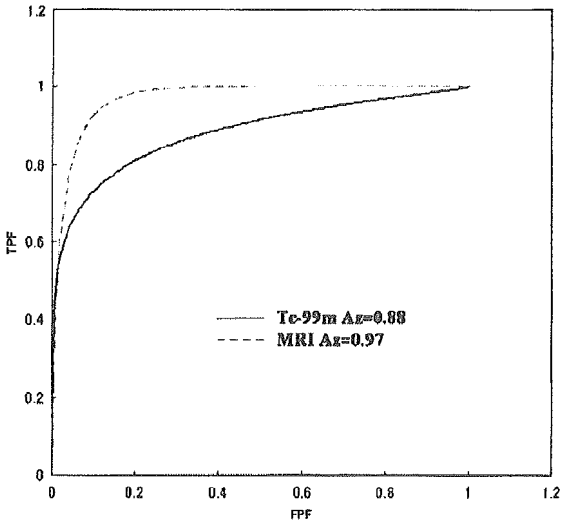

FIGURE 4. The composite receiver operating characteristic (ROC) curves of the salivary scintigram set and the magnetic resonance (MR) imaging set for the detection of Warthin tumor are shown. The average area under each composite ROC curve (Az) value of the composite ROC curves of the MR imaging set (0.97) is significantly higher than that of the salivary scintigram set (0.88). FPF indicates false-positive fraction; TPF, true-positive fraction.

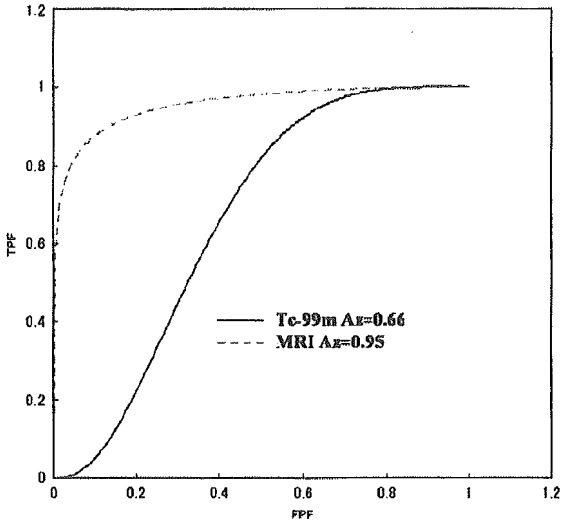

FIGURE 5. The composite receiver operating characteristic (ROC) curves of the salivary scintigram set and the magnetic resonance (MR) imaging set for the detection of malignant parotid tumor are shown. The average area under each composite ROC curve (Az) value of the composite ROC curves of the MR imaging set (0.95) is significantly higher than that of the salivary scintigram set (0.66). FPF indicates false-positive fraction; TPF, true-positive fraction.

DISCUSSION

Warthin tumor, also called adenolymphoma or papillary cystadenoma lymphomatosum, is the second most common benign tumor of the parotid gland after pleomorphic adenoma. Warthin tumor is more common in middle-aged and older men and is usually found in the parotid gland or periparotid region, mostly involving the inferior pole of the gland. It is the most common bilateral and multifocal parotid neoplasm. A Warthin tumor is usually spherical to ovoid in shape, with a smooth margin, and is commonly 2–4 cm in diameter.

The usefulness of Tc-99m pertechnetate scintigraphy with or without lemon juice stimulation in detection of Warthin tumors has been reported.[1,2] The mechanism of Tc-99m pertechnetate accumulation in Warthin tumors is thought to be attributable to the epithelial cells contained within tumors, which can extract large anions such as pertechnetate from the blood.[3] Some articles have reported cases of Warthin tumors without increased activity of Tc-99m pertechnetate, however. Yoshimura and Nohtomi[4] speculated that these Warthin tumors might have fewer active epithelial cells. Miyake et al[2] reported that there was significant correlation between tumor size and the degree of Tc-99m pertechnetate uptake after lemon juice stimulation but that there was no correlation between histologic subtype and Tc-99m uptake. The presence or absence of large cystic components in Warthin tumors is also important for interpreting the Tc-99m pertechnetate scintigram.[2] Warthin tumors without increased

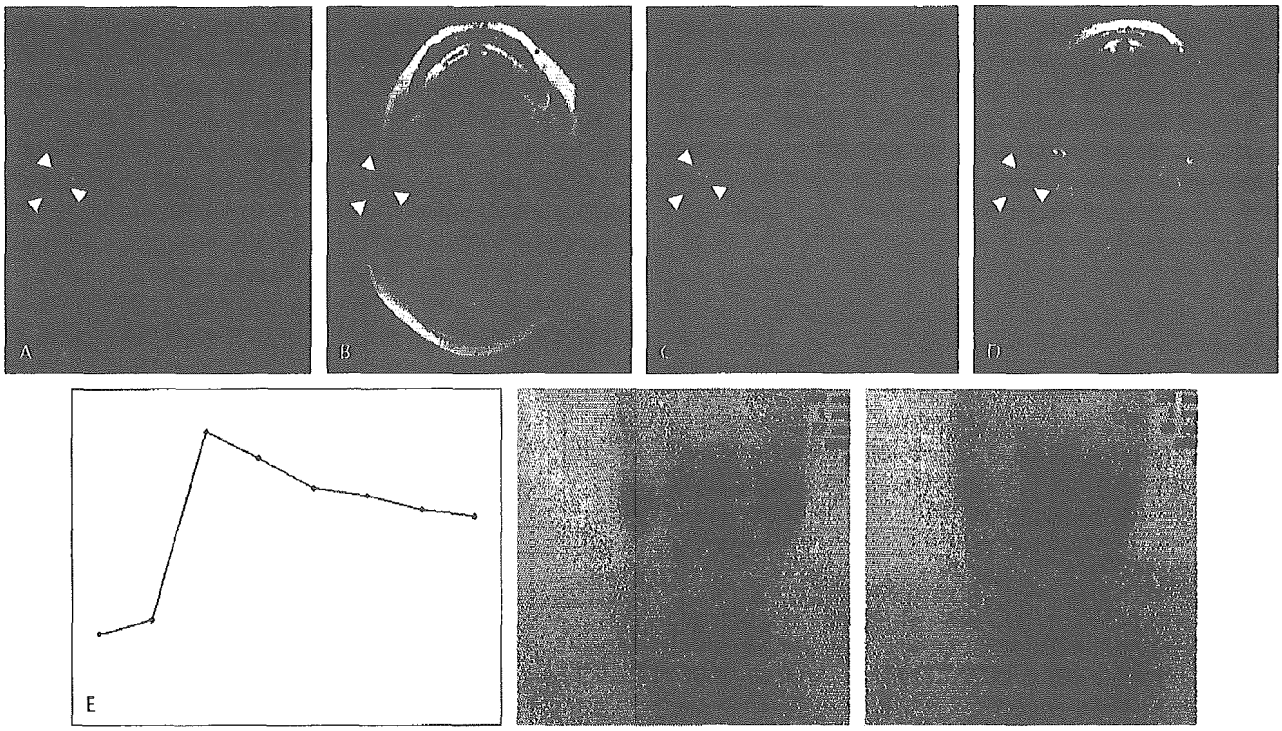

FIGURE 6. Reactive intraparotid lymphadenopathy in a 61-year-old man. A, Short inversion time inversion recovery image (repetition time/echo time [TR/TE]: 4000 milliseconds/30 milliseconds, axial plane) shows a well-defined high-intensity lesion in the inferior pole of the right parotid gland (arrowheads). B, On T1-weighted imaging (TR/TE: 420milliseconds/9 milliseconds, axial plane), the lesion shows isointensity to the right sternocleidomastoid muscle (arrowheads). C, On diffusion-weighted imaging, the lesion shows high intensity (arrowheads) and the automatically constructed apparent diffusion coefficient (ADC) map reveals an ADC value of this lesion of 063 × 10^{-3} mm^2/s, which is lower than that of the cervical spinal cord (1.08 × 10^{-3} mm^2/s). D, On fat-suppression, contrast-enhanced, T1-weighted imaging (TR/TR: 340 milliseconds/20 milliseconds, axial plane), the lesion shows slightly heterogeneous enhancement (arrowheads). E, Time-signal intensity curve, plotted from the signal intensity values obtained for the lesion on dynamic magnetic resonance imaging, shows early enhancement and a high washout ratio (41%). The early image with technetium-99m pertechnetate (F) and the late image with lemon juice stimulation (G) are negative. Salivary juice retention in the Stensen ducts (arrows) and oral cavity (arrowheads) is obtained.

activity of Tc-99m pertechnetate were the cause of the relatively low sensitivity of the scintigrams in the evaluation by Miyake et al.[2] In our study, the mean size of high-uptake Warthin tumors was 29 ± 6 mm, whereas that of low-uptake Warthin tumors, excluding large cystic components (20 ± 7 mm), was significantly ($P = 0.017$) smaller.

Recent studies have reported that MR imaging, including ADC values on DW imaging and Time-signal intensity curves on dynamic contrast-enhanced imaging, was useful for the pathologic diagnosis of parotid tumors.[13–16] Warthin tumors were usually revealed to involve the inferior pole of the parotid gland and to have a smooth margin on T1-weighted and T2-weighted imaging. Warthin tumor, epithelial stroma, and lymphoid tissue with microscopic cysts filled with a proteinous secretion showed early enhancement and a high washout ratio (≥30%) on dynamic enhanced studies and a low ADC value on DW images. A 30% washout ratio threshold tended to be useful for predicting whether salivary gland tumors were benign or malignant.[15] According to Ikeda et al,[13] the ADC values of Warthin tumors (0.96 ± 0.13 [SD] × 10^{-3} mm^2/s) were significantly lower than those of malignant tumors (1.19 ± 0.19 [SD] × 10^{-3} mm^2/s), as were the intensities of the characteristic hypointensity areas of Warthin tumors on STIR and T2-weighted images. The cellular components with accumulated microscopic cysts containing proteinous fluid with foamy cells, red cells, and neutrophils were recognized as high-intensity foci on T1-weighted images and characteristic hypointensity on STIR and T2-weighted images (see Fig. 1). The additional information on ADC, washout ratio, and TICs confirmed that the tumor was Warthin tumor.[13]

In our study, no Warthin tumor was scored as negative by the 2 readers. There were 2 false-positive cases, both reactive intraparotid lymphadenopathies, in the interpretation of the MR imaging set by the 2 readers. Warthin tumor and a reactive intraparotid lymph node are similar in their MR features. Both lesions involved the inferior pole of the parotid glands and had a smooth margin on T1-weighted and T2-weighted imaging; they also showed early enhancement and a high washout ratio (>30%) on dynamic MR images and lower ADC values than that of the spinal cord on DW images (see Figs. 1, 6). The hypointensity focus on STIR,

characteristic for Warthin tumor, although there are exceptions,[13] was not detected in the reactive lymph node (see Fig. 6). Malignant and benign parotid tumors, except for Warthin tumor, show a cold scan on Tc-99m pertechnetate scintigraphy. Small and cystic Warthin tumors also show a cold scan, however, making the differentiation of malignant from benign parotid tumors by Tc-99m pertechnetate scintigraphy difficult. Arbab et al[5] reported that a combined Tc-99m and Ga-67 citrate scan is almost specific in the diagnosis of sialoadenitis but that its usefulness in differentiating malignant from benign tumors is doubtful. In our study, detection of malignant tumors by a Tc-99m scan showed poor results, whereas satisfactory results were obtained with MR imaging (see Table 2). The average Az values of the composite ROC curves of the salivary scintigram set and the MR imaging set for malignant tumors were 0.66 and 0.94 (see Fig. 5). According to Wang et al,[14] the Az value of the ROC curve for use in differentiating malignancies from benign lesions was 0.87, with the sensitivity and specificity being 84% and 91%, respectively. They used a threshold value of 1.22×10^{-3} mm^2/s for predicting malignancy, but a reactive lymph node without macronecrosis and Warthin tumor showed low mimicked values of malignant tumors. Yabuuchi et al[15] chose a washout ratio of 30% on dynamic MR imaging to differentiate malignant from benign tumors, and the sensitivity and specificity were 89% and 78%, respectively. Ikeda et al[13] revealed that Warthin tumor has a low ADC value on DW imaging and high washout ratio on dynamic MR imaging. In our study, based on these studies, the MR imaging set showed a high Az value (0.94) in differentiating malignancies from benign lesions for malignant tumors as well as satisfactory sensitivity and specificity (see Table 2). One acinic cell carcinoma was misdiagnosed as benign because of its smooth margin and high washout ratio (33%) on dynamic MR imaging, representing 1 false-negative case, but there were no false-positive cases in the interpretation of the MR imaging set for malignant tumors.

CONCLUSIONS

Although intraparotid lymph nodes were similar to Warthin tumors and 1 malignant tumor with a smooth margin and high washout ratio on dynamic MR imaging was misdiagnosed as benign on MR imaging, traditional MR imaging with dynamic contrast-enhanced and DW imaging is a more useful method for evaluating Warthin tumor compared with Tc-99m pertechnetate scintigraphy, and it also has an advantage over Tc-99m scans in terms of differentiating malignant parotid tumors from benign tumors.

REFERENCES

1. Murata Y, Yamada I, Umehara I, et al. Diagnostic accuracy of technetium-99m-pertechnetate scintigraphy with lemon juice stimulation to evaluate Warthin's tumor. *J Nucl Med.* 1998;39:43–46.
2. Miyake H, Matsumoto A, Hori Y, et al. Warthin's tumor of parotid gland on Tc-99m pertechnetate scintigraphy with lemon juice stimulation: Tc-99m uptake, size, and pathologic correlation. *Eur Radiol.* 2001;11: 2472–2478.
3. Weinstein GS, Harvey RT, Zimmer W, et al. Technetium-99m pertechnetate salivary gland imaging: its role in the diagnosis of Warthin's tumor. *J Nucl Med.* 1994;35:179–183.
4. Yoshimura Y, Nohtomi M. Bilateral papillary cystadenoma lymphomatosum of the parotid gland without accumulation of technetium 99m pertechnetate: report of a case and review of the literature. *J Oral Maxillofac Surg.* 1991;49:401–404.
5. Arbab AS, Koizumi K, Uchiyama G, et al. The usefulness and limitations of combined Tc-99m pertechnetate and Ga-67 citrate imaging of salivary gland disorders. *Clin Nucl Med.* 1995;20:5–12.
6. Sostre S, Medina L, de Arellano GR. The various scintigraphic patterns of Warthin's tumor. *Clin Nucl Med.* 1987;12:620–626.
7. Higashi T, Murahashi H, Ikuta H, et al. Identification of Warthin's tumor with technetium-99m pertechnetate. *Clin Nucl Med.* 1987;12:796–800.
8. Donovan DT, Conley JJ. Capsular significance in parotid tumor surgery: reality and myths of lateral lobectomy. *Laryngoscope.* 1984;94:324–329.
9. Dykun RJ, Deitel M, Borowy ZJ, et al. Treatment of parotid neoplasms. *Can J Surg.* 1980;23:14–19.
10. Hee CG, Perry CF. Fine-needle aspiration cytology of parotid tumours: is it useful? *Aust NZ J Surg.* 2001;71:345–348.
11. Zbaren P, Schar C, Hotz MA, et al. Value of fine-needle aspiration cytology of parotid gland masses. *Laryngoscope.* 2001;111:1989–1992.
12. Flezar M, Pogacnik A. Warthin's tumour: unusual vs. common morphological findings in fine needle aspiration biopsies. *Cytopathology.* 2002; 13:232–241.
13. Ikeda M, Motoori K, Hanazawa T, et al. Warthin tumor of the parotid gland: diagnostic value of MR imaging with histopathologic correlation. *AJNR Am J Neuroradiol.* 2004;25:1256–1262.
14. Wang J, Takashima S, Takayama F, et al. Head and neck lesions: characterization with diffusion-weighted echo-planar MR imaging. *Radiology.* 2001;220:621–630.
15. Yabuuchi H, Fukuya T, Tajima T, et al. Salivary gland tumors: diagnostic value of gadolinium-enhanced dynamic MR imaging with histopathologic correlation. *Radiology.* 2003;226:345–354.
16. Motoori K, Yamamoto S, Ueda T, et al. Inter- and intratumoral variability in magnetic resonance imaging of pleomorphic adenoma: an attempt to interpret the variable magnetic resonance findings. *J Comput Assist Tomogr.* 2004;28:233–246.

Int J Clin Oncol (2005) 10:201–203
DOI 10.1007/s10147-004-0471-8

CASE REPORT

Koichi Isobe · Takashi Uno · Takashi Aruga
Hiroyuki Kawakami · Naoyuki Ueno
Toyoyuki Hanazawa · Yoshitaka Okamoto · Hisao Ito

Weekly cisplatin administration concurrent with radiation therapy for locoregionally advanced nasopharyngeal carcinoma

Received: September 3, 2004 / Accepted: December 10, 2004

Abstract Radiation therapy (RT) with concurrent and adjuvant chemotherapy has been a widely accepted treatment for patients with locoregionally advanced nasopharyngeal carcinoma (NPC). We administered 40 mg/m^2 cisplatin (CDDP) weekly, concurrently with RT, to six consecutive patients with locoregionally advanced NPC to evaluate its toxicity and efficacy. The median number of courses of CDDP administration was 4.5 and the median radiation dose was 69.7 Gy. Grade 3 leukopenia was observed in three patients. All but one patient experienced grade 3 or 4 skin reactions, pharyngitis, or dysphagia. All but one patient achieved a complete response, and the remaining patient received radical neck dissection for persistent cervical lymphadenopathies, which contained no cancer cells. All six patients were disease-free at last contact, with a median follow up of 23.5 months. This regimen is well tolerated in patients with locoregionally advanced NPC.

Key words NPC · Concurrent chemoradiotherapy · Weekly CDDP · Intergroup Study 0099

Introduction

Concurrent chemoradiotherapy is the mainstay of treatment for various malignancies.[1–4] Platinum agents, including cisplatin (CDDP), with or without other agents, are used commonly in this setting; however, an optimal CDDP administration schedule remains to be determined. In patients with nasopharyngeal cancer (NPC), the Intergroup Study 0099 (IGS) has demonstrated significant results by administering 100 mg/m^2 CDDP concurrent with radiation therapy (RT) at 3-week intervals.[5,6] After the publication of the IGS, we attempted to adopt an identical combined modality treatment for patients with locoregionally advanced NPC, between March 2001 and June 2002. Although we treated only three patients according to the this regimen, we failed to demonstrate its feasibility and efficacy, because of its severe acute adverse events, poor compliance, and unsatisfactory outcome.[7]

In contrast to the IGS, a Hong Kong group conducted a phase III randomized trial comparing radical RT with concurrent weekly CDDP and RT.[8] They demonstrated significant improvement of progression-free survival in patients with advanced stages, with 40 mg/m^2 weekly CDDP administration. We report the feasibility and efficacy of this weekly chemotherapy CDDP schedule, given concurrently with RT.

Case report

From July 2002, we have treated six consecutive patients with biopsy-proven stage IIB to IVB NPC. All six patients met the inclusion criteria of Chan et al.,[8] and underwent a complete history, physical examination, complete blood counts, screening blood tests of hepatic and renal function, and 3 consecutive days of 24-h creatinine clearance. The disease evaluation included a chest radiograph; bone scintigraphy; computed tomography (CT) of the head and neck, chest, and abdomen; magnetic resonance imaging (MRI) of the nasopharynx and base of skull; and fiberoptic endoscopy and biopsy of the nasopharynx. The patients were staged according to the 1997 International Union Against Cancer (UICC)-TNM staging system. The patients' characteristics are shown in Table 1. Informed consent was provided according to the Declaration of Helsinki.

The patients received 40 mg/m^2 CDDP weekly during RT, starting on the first day of RT. All patients received adequate hydration and a serotonin antagonist against emesis during the CDDP administration. Chemotherapy was

K. Isobe (✉) · T. Uno · T. Aruga · H. Kawakami · N. Ueno · H. Ito
Department of Radiology, Chiba University Hospital, 1-8-1 Inohana, Chuo-ku, Chiba 260-8677, Japan
Tel. +81-43-226-2100; Fax +81-43-226-2101
e-mail: isobeko@ho.chiba-u.ac.jp

T. Hanazawa · Y. Okamoto
Department of Otorhinolaryngology, Chiba University Hospital, Chiba, Japan

delayed until bone marrow suppression recovered, and was suspended if serum creatinine was greater than 1.5 mg/dl, and/or creatinine clearance fell to less than 50 ml/min. No patients were scheduled to receive adjuvant and/or neoadjuvant chemotherapy.

With regard to RT, CT-based treatment planning was used to assess the extent of the primary tumor and the neck nodes. The nasopharynx and the upper neck were treated with two opposed lateral fields. A separate anterior supraclavicular field was used to irradiate the lower neck and supraclavicular fossa. The patients were treated with a combination of 4- and 10-MV photons to achieve dose homogeneity. An electron field of appropriate energy was also applied to treat posterior neck nodes after sparing the spinal cord. The fractional daily dose was 2 Gy, with a planned total dose of 66 Gy.

The response assessment included physical examination, fiberoptic endoscopy, and CT and/or MRI of the nasopharynx and neck, and responses were classified according to the *New guidelines to evaluate the response to treatment in solid tumors*.[9] Acute toxicities were graded according to the National Cancer Institute common toxicity criteria.

All six patients received RT without treatment breaks, with a median dose of 69.7 Gy (range, 64 to 70 Gy). Chemotherapy was delivered in three to six weekly courses, with a median course number of 4.5. The reasons for suspension of CDDP administration included renal toxicity in two patients, and grade 3 leukopenia, pharyngitis, and patient refusal in 1 patient each. The acute toxicity profiles are shown in Table 2. Although three patients developed grade 3 leukopenia, the other hematological toxicities were well tolerated. However, all but one patient experienced grade 3 or 4 skin reactions, pharyngitis, or dysphagia. Body weight loss ranged from 4% to 20.7%, with a median of 14.5%. At the end of the treatment, five patients achieved a complete response, and the remaining patient obtained a partial response; this patient received radical neck dissection for persistent lymphadenopathies; however, histopathological examination revealed no cancer cells in the surgical specimens. All six patients were alive without disease at last contact, with a median follow up of 23.5 months (range, 13 to 27 months).

Table 1. Patient characteristics

	Age (years)	Sex	TNM	Histology
Case 1	49	Male	T4N2M0	WHO III
Case 2	20	Male	T1N3bM0	WHO III
Case 3	59	Male	T4N0M0	WHO III
Case 4	62	Female	T3N2M0	WHO II
Case 5	65	Female	T3N1M0	WHO III
Case 6	74	Male	T2bN1M0	WHO II

Discussion

Concurrent chemoradiotherapy with adjuvant chemotherapy has become standard practice following the publication of excellent results by the IGS.[5,6] Subsequently, several phase II or III studies have demonstrated encouraging results with regard to concurrent chemoradiotherapy with or without adjuvant or neoadjuvant chemotherapy.[8,10–15] In the IGS, patients in the experimental arm received 100 mg/m^2 CDDP as a single agent at 3-week intervals, concurrently with radical RT. In four other studies, patients were also administered 100 mg/m^2 CDDP as a single agent, at 3- or 5-week intervals, concurrently with RT;[10–13] in two of these studies, the CDDP dose was divided equally and given on 4 or 5 consecutive days.[12,13] In our previous study, three patients were to receive the IGS regimen; however, they were not able to complete their planned chemotherapy because of its severe acute adverse events.[7]

In contrast, Chan et al.[8] examined the efficacy of weekly administration of 40 mg/m^2 CDDP concurrently with RT (66 Gy/6.5 week), compared with RT alone, in a randomized phase III trial. They demonstrated that progression-free survival was significantly prolonged in patients with advanced stage disease; however, in the overall comparison, progression-free survival was not different among the treatment arms. This CDDP administration schedule has been shown to have acceptable toxicities, with an encouraging outcome for cervical cancer,[2] and, in light of our previous experiences employing the IGS protocol, we incorporated weekly CDDP administration into the present study. Although, in comparison to our previous study, hematological toxicities were more frequent in the present one, nonhematological toxicities were comparable to those in the previous study,[7] and we obtained encouraging results in the present study.

Table 2. Acute adverse events; maximum grade observed for each patient

	Case 1 Grade	Case 2 Grade	Case 3 Grade	Case 4 Grade	Case 5 Grade	Case 6 Grade
Leukopenia	2	3	1	3	3	1
Anemia	1	1	1	2	3	1
Thrombocytopenia	1	1	1	1	0	0
Weight loss	2 (−13.5%)	2 (−18.8%)	2 (−10.7%)	2 (−15.6%)	0 (−4%)	3 (−20.7%)
Dermatitis	2	2	3	3	2	2
Dysphagia	3	3	2	2	2	3
Pharyngitis	3	4	2	3	2	3

Another concurrent chemoradiotherapy schedule includes daily administration of chemotherapy. This schedule has not been tested in head and neck cancers, including NPC; however, Schaake-Koning et al.[16] demonstrated that 6 mg/m^2 CDDP given daily, in combination with RT, in patients with inoperable non-small-cell lung cancer, improved the survival and local control rates compared with 30 mg/m^2 weekly administration. It is still to be determined whether the same situation would apply in patients with NPC or other head and neck cancers.

Little is known about whether combination chemotherapy is superior to CDDP monochemotherapy in the setting of concurrent chemoradiotherapy. Standard chemotherapy for head and neck cancers is a combination of CDDP and 5-fluorouracil (5-FU). Patients with stage II to IV NPC received concurrent chemoradiotherapy consisting of CDDP plus 5-FU in a Taiwan group study, and it was concluded that concurrent chemoradiotherapy with adjuvant chemotherapy would be the best standard strategy for intermediate-risk patients.[14] Recently, Lin et al.[15] have also demonstrated, in a phase III trial, that concurrent chemoradiotherapy, consisting of 80 mg/m^2 CDDP and 1600 mg/m^2 5-FU as a 96-h continuous infusion, given at 4-week intervals, significantly improved both overall survival and progression-free survival, with acceptable toxicities. However, in patients with cervical cancer, a Gynecologic Oncology Group study failed to demonstrate a survival benefit for a CDDP plus 5-FU regimen compared with weekly CDDP administration, and the combined regimen showed more hematological and gastrointestinal toxicities.[17] Whether the addition of 5-FU to CDDP is more effective than CDDP monochemotherapy for NPC remains to be elucidated. The optimal chemotherapy regimen and appropriate administration schedule, regarding concurrent RT and chemotherapy for the management of locoregionally advanced NPC, remain to be established in future clinical studies. Furthermore, the efficacy and toxicities of new active agents against NPC, such as docetaxel and gemcitabine, remain to be evaluated.[18,19]

In summary, although both our previous[7] and present studies were too small to draw any conclusions, we have suggested that, for CDDP monochemotherapy in a concurrent RT setting, weekly 40 mg/m^2 administration is superior to 100 mg/m^2 delivery at 3-week intervals for Japanese patients with locoregionally advanced NPC, with respect to both efficacy and toxicity profiles. We will extend our experience employing a weekly CDDP administration schedule for the management of locoregionally advanced NPC. We will also incorporate adjuvant chemotherapy to eliminate microscopic metastatic disease in a future prospective trial.

References

1. Spira A, Ettinger DS (2004) Multidisciplinary management of lung cancer. N Engl J Med 350:379–392
2. Loizzi V, Cormio G, Loverro G, et al. (2003) Chemoradiation: a new approach for the treatment of cervical cancer. Int J Gynecol Cancer 13:580–586
3. Wu PC, Posner MC (2003) The role of surgery in the management of oesophageal cancer. Lancet Oncol 4:481–488
4. Al-Sarraf M (2002) Treatment of locally advanced head and neck cancer: historical and critical review. Cancer Control 9:387–399
5. Al-Saraf M, LeBlanc M, Giri PG, et al. (1998) Chemoradiotherapy versus radiotherapy in patients with advanced nasopharyngeal cancer: phase III randomized Intergroup Study 0099. J Clin Oncol 16:1310–1317
6. Al-Saraf M, LeBlanc M, Giri PG, et al. (2001) Superiority of 5-year survival with chemo-radiotherapy (CT-RT) vs radiotherapy in patients (Pts) with locally advanced nasopharyngeal cancer (NPC). Intergroup (0099) (SWOG 8892, RTOG 8817, ECOG 2388) phase III study: final report (abstract no. 905). Proc Am Soc Clin Oncol 20:227a
7. Isobe K, Kawakami H, Uno T, et al. (2003) Concurrent chemoradiotherapy for locoregionally advanced nasopharyngeal carcinoma: is Intergroup Study 0099 feasible in Japanese patients? Jpn J Clin Oncol 33:497–500
8. Chan ATC, Teo PML, Ngan RK, et al. (2002) Concurrent chemotherapy-radiotherapy compared with radiotherapy alone in locoregionally advanced nasopharyngeal carcinoma: a progression free survival analysis of a phase III randomized trial. J Clin Oncol 20:2038–2044
9. Therasse P, Arbuck SG, Eisenhauer EA, et al. (2000) New guidelines to evaluate the response to treatment in solid tumors. J Natl Cancer Inst 92:205–216
10. Wolden SL, Zelefsky MJ, Kraus DH, et al. (2001) Accelerated concomitant boost radiotherapy and chemotherapy for advanced nasopharyngeal carcinoma. J Clin Oncol 19:1105–1110
11. Chua DTT, Sham JST, Au GKH (2004) Concurrent chemoirradiation with cisplatin followed by adjuvant chemotherapy with ifosfamide, 5-fluorouracil, and leucovorin for stage IV nasopharyngeal carcinoma. Head Neck 26:118–126
12. Rischin D, Corry J, Smith J, et al. (2002) Excellent disease control and survival in patients with advanced nasopharyngeal cancer treated with chemoradiation. J Clin Oncol 20:1845–1852
13. Tan EH, Chua ET, Wee J, et al. (1999) Concurrent chemoradiotherapy followed by adjuvant chemotherapy in Asian patients with nasopharyngeal carcinoma: toxicities and preliminary results. Int J Radiat Oncol Biol Phys 45:597–601
14. Cheng SH, Yen KL, Jian JJM, et al. (2001) Examining prognostic factors and patterns of failure in nasopharyngeal carcinoma following concomitant radiotherapy and chemotherapy: impact on future clinical trials. Int J Radiat Oncol Biol Phys 50:717–726
15. Lin JC, Jan JS, Hsu CY, et al. (2003) Phase III study of concurrent chemoradiotherapy versus radiotherapy alone for advanced nasopharyngeal carcinoma: positive effect on overall and progression-free survival. J Clin Oncol 21:631–637
16. Schaake-Koning C, Bogaert W, Dalesio O, et al. (1992) Effects of concomitant cisplatin and radiotherapy on inoperable non-small-cell lung cancer. N Engl J Med 326:524–530
17. Rose PG, Bundy BN, Watkins EB, et al. (1999) Concurrent cisplatin-based radiotherapy and chemotherapy for locally advanced cervical cancer. N Engl J Med 340:1144–1153
18. Ngan RKC, Yiu HHY, Lau WH, et al. (2002) Combination gemcitabine and cisplatin chemotherapy for metastatic or recurrent nasopharyngeal carcinoma: report of a phase II study. Ann Oncol 13:1252–1258
19. Johnson FM, Garden A, Palmer JL, et al. (2004) A phase II study of docetaxel and carboplatin as neoadjuvant therapy for nasopharyngeal carcinoma with early T status and advanced N status. Cancer 100:991–998

Jpn J Clin Oncol 2005;35(3)116–120
doi:10.1093/jjco/hyi041

Hyperfractionated Radiation Therapy for Locoregionally Advanced Nasopharyngeal Cancer

Koichi Isobe[1], Takashi Uno[1], Hiroyuki Kawakami[1], Naoyuki Ueno[1], Takashi Aruga[1], Shigeo Yasuda[1], Toyoyuki Hanazawa[2], Yoshitaka Okamoto[2], Hisao Ito[1] and Naoyuki Shigematsu[3]

Departments of [1]Radiology and [2]Otorhinolaryngology, Chiba University Hospital, Chiba and [3]Department of Radiology, Keio University, School of Medicine, Tokyo, Japan

Received November 9, 2004; accepted January 2, 2005

Objective: The purpose of this study is to clarify the efficacy and toxicity of hyperfractionated radiation therapy (RT) for patients with nasopharyngeal cancer (NPC).
Methods: Twenty-two patients with NPC treated at our hospital between April 1994 and December 2002 were the subjects of this study. They received hyperfractionated RT with a fraction size of 1.2 Gy, with a median tumor dose of 72 Gy (range 64.8–80.4). During this study period, our institutional strategy for locoregionally advanced NPC included neoadjuvant or concurrent chemotherapy combined with hyperfractionated RT, and 17 patients received some forms of cisplatin-containing chemotherapy.
Results: With a median follow-up of 59 months, the estimated 5-year disease-free survival rate and overall survival rate were 72.7 and 85.2%, respectively. Acute hematological toxicities were acceptable and manageable. However, >50% of patients required nutritional support, and experienced severe pharyngitis, skin reaction and body weight loss. With regard to late sequelae, one patient developed grade 3 osteomyelitis, and one patient each developed grade 4 passage disturbance and laryngeal edema. No patients experienced any grades of optic nerve injury or temporal lobe necrosis.
Conclusions: Hyperfractionated RT using 1.2 Gy per fraction, for a total dose of 72 Gy, produces a comparable treatment outcome. Although deleterious neurological sequelae were not observed in this study, caution should be exercised regarding other late sequelae, such as osteomyelitis and passage disturbance.

Key words: nasopharyngeal cancer (NPC) – hyperfractionation – altered fractionation – late effect

INTRODUCTION

Radiation therapy (RT) has long been a primary treatment of choice for patients with non-metastatic nasopharyngeal carcinoma (NPC). However, significant numbers of patients with locoregionally advanced disease develop recurrence above the clavicle and distant metastasis. As NPC is not only a radiosensitive tumor but also a chemosensitive one, several investigators have incorporated chemotherapy into the management of NPC in an attempt to improve both the local control rate and survival probability (1–4). As a result, concurrent chemoradiotherapy with adjuvant chemotherapy improved survival, but randomized studies have not supported the use of neoadjuvant or adjuvant chemotherapy (1–6).

For reprints and all correspondence: Koichi Isobe, 1-8-1 Inohana, Chuo-ku, Chiba 260-8677, Japan. E-mail: isobeko@ho.chiba-u.ac.jp

In contrast, several researchers have tried to deliver a higher radiation dose, without increasing late complications, to improve the local control rate and survival probability. One of these contrivances is the application of a hyperfractionated RT schedule. The rationale for hyperfractionation is based on exploiting differences in the radiobiology of the tumor and late responding tissues (7). The observations that late responding normal tissues show greater repair of non-lethal injury between dose fractions than do tumor cells, and tumor cells in the radioresistant phase of the cell cycle are redistributed into the more radiosensitive phase between dose fractions, enabled the increase of the relative biological dose to the tumor. The recent large RTOG (Radiation Therapy Oncology Group) randomized controlled trial demonstrated that both hyperfractionation and accelerated fractionation with the concomitant boost technique were superior to standard fractionation in terms of locoregional control and disease-free survival (8). Although NPC shows a somewhat different clinical behavior from other head and neck cancers and is usually dealt with

separately, a similar strategy has been applied for locoregionally advanced NPC, increasing the total dose to the tumor without increasing late complications, through hyperfractionation (9–16). Here we report our experience with hyperfractionated RT for patients with NPC.

PATIENTS AND METHODS

PATIENT CHARACTERISTICS

Between April 1994 and December 2000, 22 consecutive patients with locoregionally advanced NPC treated at our hospital by hyperfractionation were the subjects of this study. There were 17 males and five females, of ages ranging from 35 to 78 years with a median age of 54 years. Histological examinations according to the World Health Organization (WHO) classification revealed that nine cases were WHO II, and 12 were WHO III. Detailed patient characteristics are listed in Table 1. Pre-treatment evaluation included a complete history and physical examination with fiberoptic endoscopy, chest radiographs, computed tomography (CT) of the head and neck, chest and abdomen, magnetic resonance imaging (MRI) of the nasopharynx and base of the skull, and bone scintigraphy. All patients had a biopsy from the nasopharynx to confirm the diagnosis. Laboratory studies included complete blood counts, blood chemistry with hepatic and renal function tests, and urinalysis. Patients receiving chemotherapy also had three consecutive days of 24 h creatinine clearance. All patients were restaged using the 1997 UICC-TNM staging system, and their stage distributions are indicated in Table 1. All but one patient had stage IIB or more advanced disease.

TREATMENT

RT therapy was delivered with a combination of 4 and 10 MV photons to achieve dose homogeneity. An appropriate energy of the electron field was also applied to treat the posterior neck node after sparing the spinal cord. The treatment volume included the primary tumor site and the neck nodes above the clavicle. The nasopharynx and the upper neck were treated with two opposed lateral fields. A separate anterior supraclavicular field was used to irradiate the lower neck and supraclavicular fossa. The fractional dose was 1.2 Gy, two fractions per day, and at least a 6 h interval between dose fractions with a planned dose of 72 Gy. The typical irradiation fields and dose distributions are shown in Fig. 1.

Table 1. Patient characteristics

No. of patients	22
Sex (male/female)	17/5
Age, *median (range)*	54 years (35–78)
Histology (WHO I/II/III)	1/9/12
T stage (T1/2a/2b/3/4)	9/2/5/4/2
N stage (N0/1/2/3a/3b)	3/4/11/2/2
Stage (I/IIA/IIB/III/IVA/IVB)	1/0/5/10/2/4

The median tumor dose was 72 Gy (range 64.8–80.4). Seventeen patients (77%) received 72 Gy in 60 fractions of RT, three received <70 Gy, and the remaining two received 75.6 and 80.4 Gy, respectively. The median total treatment time during RT was 45 days (range 39–54).

During this study period, our institutional strategies in the management of NPC included neoadjuvant and/or concurrent chemotherapy; however, the decision regarding whether chemotherapy would be given depended solely on the discretion of the treating physician. Although five patients did not receive any form of chemotherapy, 11 received chemotherapy concurrently with RT (CRT group). Of these 11 patients, three also received neoadjuvant chemotherapy. Of the remaining six patients, two received both neoadjuvant and adjuvant chemotherapy, and four received neoadjuvant chemotherapy exclusively. Adjuvant or neoadjuvant chemotherapy consisted of a combination of 100 mg/m^2 of cisplatin (CDDP) and 1500 mg/m^2 of 5-fluorouracil for 5 days. In a concurrent setting, five patients received 70–100 mg/m^2 of CDDP in a triweekly schedule, three received 5 or 6 mg/m^2 of daily CDDP administration, and the remaining three received 100 mg/m^2 of weekly carboplatin (CBDCA).

Acute toxicities were graded according to the National Cancer Institute common toxicity criteria version 2.0. Late toxicities were recorded according to the RTOG scale as long as this was feasible. The Kaplan–Meier method was used to calculate survival probability (17). Informed consent was provided according to the Declaration of Helsinki.

RESULTS

At the time of this analysis, 17 patients were alive with a median follow-up of 59 months (range 34–106). The estimated 5-year locoregional control rate (LCR), disease-free survival and overall survival rates were 80.2% [95% confidence interval (CI), 62.8–97.6], 72.7% (95% CI, 54.1–91.3) and 85.2% (95% CI, 69.6–100), respectively (Fig. 2). The 5-year LCR in the CRT group was 80% (95% CI, 55–100). However, it was 81% (95% CI, 57–100) among patients who did not receive concurrent chemotherapy (non-CRT group). Four patients experienced in-field recurrence, two of whom died of their disease, and the remaining two were alive after salvage operations. Two patients with intercurrent disease and one patient who developed liver metastasis also died.

The acute toxicity profiles other than hematological adverse events are listed in Table 2. Two patients experienced grade 3 leukopenia, but no patients developed more than grade 2 anemia or thrombocytopenia. Nineteen patients suffered from grade 3 skin reaction and/or pharyngitis, and the median body weight loss was 11.8% (range 1.6–24.0). As shown in Table 2, the severity of acute adverse events was not related to the concurrent chemotherapy. With regard to late complications, grade 2 and 3 xerostomia occurred in 10 (45%) and three (14%) patients, respectively. Furthermore, three patients experienced more than grade 2 sequelae. One patient developed grade 3 osteomyelitis of the mandible,

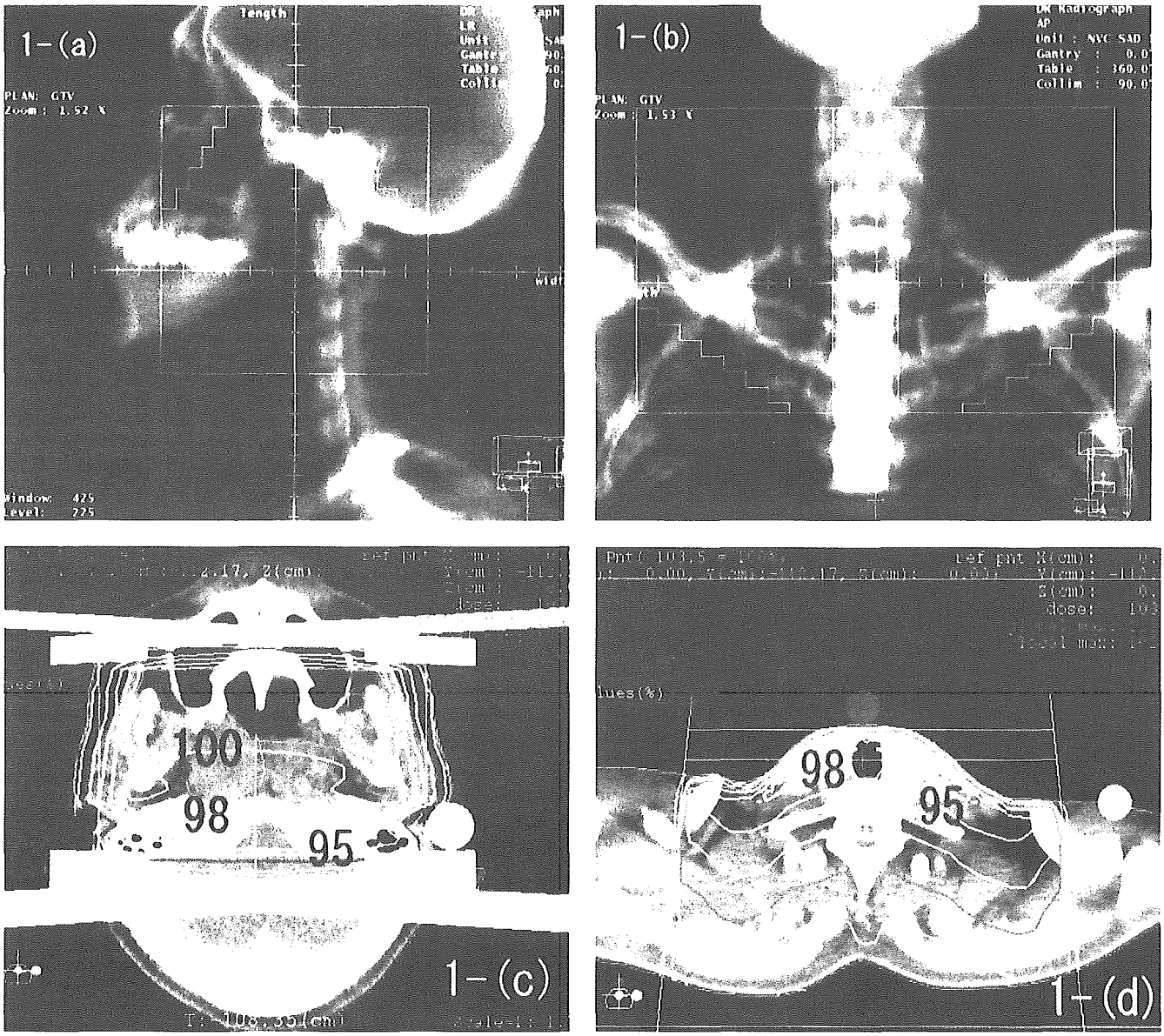

Figure 1. Typical irradiation field and dose distribution. Irradiation field for upper neck (a) and lower neck (b). Dose distribution at the level of the nasopharynx (c), and supraclavicular fossa (d).

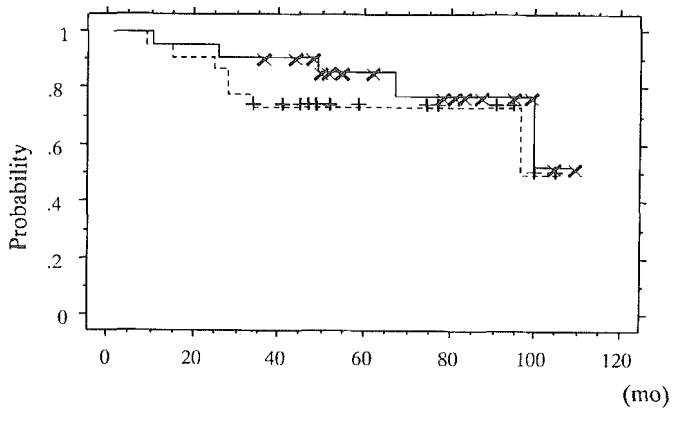

Figure 2. Overall survival curve (solid line) and disease-free survival curve (dashed line).

Table 2. Acute adverse events other than hematological toxicity

Toxicity	No. of patients (%)	
	CRT	Non-CRT
Pharyngitis (grade 3 and 4)	8 (73)	5 (45)
Skin reaction (grade 3 and 4)	9 (82)	9 (82)
Nutrition (grade 3)	8 (73)	7 (64)
Body weight loss (grade 2 and 3)	8 (73)	4 (36)

CRT, chemoradiotherapy.

one required gastrostomy for nutritional support (grade 4) and one underwent tracheostomy for persistent laryngeal edema (grade 4). These three patients received a total dose of 72, 72 and 75.6 Gy, respectively. No patients experienced optic

nerve injury, symptomatic temporal lobe necrosis or treatment-related death. The total dose to the temporal lobe ranged from 49.1 to 75.6 Gy with a mean dose of 70.7 Gy.

DISCUSSION

External beam RT is the standard treatment for patients with NPC; however, many patients with advanced disease suffer from local recurrence. As local control is prognostically important in NPC, various attempts have been made to improve local control probability by delivering higher radiation doses. These strategies include the addition of intracavitary brachytherapy, three-dimensional conformal RT, intensity modulated RT (IMRT) and hyperfractionated RT (9–16), which would enable us to administer higher doses without an apparent increase in late normal tissue sequelae. In a review with regard to altered fractionated RT for head and neck cancer (18), Nguyen and Ang concluded that the use of three fractions per day without total dose reduction produces a significantly higher frequency of late normal tissue complications; however, a modest acceleration of RT by 1 week without total dose reduction, a break in treatment by giving six fractions of 2 Gy per week or by a concomitant boost regimen, or an acceleration of RT by >3 weeks with total dose reduction of 6–7 Gy (10%) improved locoregional control without much increase in the late toxic effect. Moreover, they stated that hyperfractionated RT is better than standard fractionation for advanced head and neck carcinoma, and that reduction of the fraction size from 2 to 1.1–1.2 Gy permits a 7–17% escalation in total doses without leading to a detectable increase in late normal tissue injury.

Similar to other head and neck cancers, several investigators have applied hyperfractionated or accelerated hyperfractionated RT for the treatment of locoregionally advanced NPC to improve locoregional control probability. Jian et al. (16) evaluated the efficacy of hyperfractionated RT using 1.2 Gy per fraction for locally advanced NPC patients with base of skull or intracranial invasion. They administered a total dose of 74.4 Gy in 62 fractions concurrently with chemotherapy. They also gave adjuvant chemotherapy thereafter, and demonstrated a 3-year LCR of 93%. For T4 patients, the 3-year LCR was 91%, and they concluded that hyperfractionation achieved excellent local control and improved survival with acceptable and reversible toxicities. Jen et al. (15) also suggested that NPC patients can be safely treated using a 1.2 Gy twice daily program with a 6 h interval up to 80 Gy. The results of these two studies were well in accordance with those of our present study, which demonstrated that a 1.2 Gy hyperfractionated RT schedule for locoregionally advanced NPC produced promising outcomes without an increase in late normal tissue complications.

In contrast, a group from the Prince of Wales Hospital (PWH) first warned that accelerated hyperfractionation caused an unexpectedly high incidence of temporal lobe necrosis in patients with NPC (9). They reported that the incidence of temporal lobe injury was 35% at 2–3.5 years after hyperfractionated RT. They used a fraction size of 1.6 Gy to a total dose of 67.2 Gy, which was devised at Massachusetts General Hospital (MGH); however, the MGH group reported that no patient developed major neurological complications (13). In an update report in 1999 (10), the PWH group speculated that the discrepancy between the MGH group results and their experience was derived from the marked difference in delineating the target volume. In a final report from the PWH (11), they concluded that accelerated hyperfractionation when used in conjunction with a two-dimensional RT planning technique resulted in increased radiation damage to the central nervous system without significant improvement in efficacy. In response to a commentary from the PWH group, a Turkish group also abandoned hyperfractionated RT using the concomitant boost technique, because they also observed severe neural complications including temporal lobe necrosis and optic neuropathy (12). Jen et al. (14,15), who have accepted hyperfractionated RT using 1.2 Gy per fraction, also warned that an accelerated hyperfractionation schedule using 1.6 Gy per fraction led to a high incidence (27%) of temporal lobe necrosis. These reports suggest that accelerated hyperfractionation employing a fraction size of 1.6 Gy would result in a significant increase in late neurological toxicities.

No reports documented severe late sequelae other than damage to the central nervous system. Although we did not experience clinically detectable late optic nerve injury or temporal lobe necrosis, we encountered two patients who developed grade 4 late complications. As the PWH group have suggested, we have to seek to reduce the risk of late normal tissue toxicities by delineating the target volume carefully. The present study demonstrated that hyperfractionated RT using 1.2 Gy per fraction could produce a comparable outcome with acceptable and manageable acute toxicities, and we conclude that 1.2 Gy per fraction of hyperfractionated RT, for a total dose of 72 Gy, would be an acceptable treatment for locoregionally advanced NPC.

References

1. Chua DTT, Sham JST, Choy D, Kwong DLW, Au GKH, Kwong PWK, et al. Patterns of failure after induction chemotherapy and radiotherapy for locoregionally advanced nasopharyngeal carcinoma: the Queen Mary Hospital experience. *Int J Radiat Oncol Biol Phys* 2001;49:1219–28.
2. Ma J, Mai HQ, Hong MH, Min HQ, Mao ZD, Cui NJ, et al. Results of a prospective randomized trial comparing neoadjuvant chemotherapy plus radiotherapy with radiotherapy alone in patients with locoregionally advanced nasopharyngeal carcinoma. *J Clin Oncol* 2001;19:1350–7.
3. Chan ATC, Teo PML, Leung TWT, Leung SF, Lee WY, Yeo W, et al. A prospective randomized study of chemotherapy adjunctive to definitive radiotherapy in advanced nasopharyngeal carcinoma. *Int J Radiat Oncol Biol Phys* 1995;33:569–77.
4. Rossi A, Molinari R, Boracchi P, Del Vecchio M, Marubini E, Nava M, et al. Adjuvant chemotherapy with vincristine, cyclophosphamide, and doxorubicin after radiotherapy in local–regional nasopharyngeal cancer: results of a 4-year multicenter randomized study. *J Clin Oncol* 1988;6:1401–10.
5. Al-Saraf M, LeBlanc M, Giri PGS, Fu KK, Cooper J, Vuong T, et al. Chemoradiotherapy versus radiotherapy in patients with advanced nasopharyngeal cancer: phase III randomized Intergroup Study 0099. *J Clin Oncol* 1998;16:1310–7.